ELSEVIER

Chemical Geology 194 (2003) 51–79

CHEMICAL GEOLOGY
INCLUDING
ISOTOPE GEOSCIENCE

www.elsevier.com/locate/chemgeo

Oil-bearing CO_2–CH_4–H_2O fluid inclusions: oil survival since the Palaeoproterozoic after high temperature entrapment

A. Dutkiewicz[a,*], J. Ridley[b], R. Buick[c]

[a] School of Geosciences, University of Sydney, Sydney, NSW 2006, Australia
[b] GEMOC, Department of Earth and Planetary Sciences, Macquarie University, Sydney, NSW 2109, Australia
[c] Department of Earth and Space Sciences and Astrobiology Program, University of Washington, Box 351310, Seattle, WA 98195-1310, USA

Received 17 December 2001; received in revised form 20 May 2002

Abstract

The 2.45-Ga fluvial quartz arenites and conglomerates of the Matinenda Formation at Elliot Lake, Canada, contain evidence for two episodes of oil migration with entrapment of oil-bearing fluid inclusions. The first episode was during diagenesis, the second during a subsequent sub-greenschist facies metamorphic event at ca. 2.2 Ga at temperatures exceeding 250 °C. Remnants of the migrating hydrocarbon fluids are preserved as radiogenic pyrobitumen nodules occupying former inter-granular pore spaces and as complex fluorescing oil-bearing fluid inclusions. The latter include two dominant types: (1) aqueous-oil inclusions with a minor oil phase, located within original detrital grains and clasts and within rare quartz overgrowths, and (2) aqueous–carbonic inclusions with a minor oil phase, light hydrocarbons and solids, located within microfractures in detrital quartz grains and clasts. The majority of Type 1 inclusions were trapped with a high salinity fluid (up to 25 wt.% NaCl equivalent) at relatively low temperatures between 80 and 200 °C and pressures of less than 2 kbar early in the burial history of the Matinenda Formation. Type 2 inclusions were trapped during metamorphism with a much lower salinity aqueous–carbonic fluid (1.2 to 17 wt.% NaCl equivalent) at temperatures between 280 and 350 °C and pressures between 1 and 1.5 kbar. Under these conditions oil may have been miscible in the mixed fluid. $\delta^{13}C$ of −25.5‰ and −24.9‰ for the pyrobitumen nodules and fluid inclusion hydrocarbon gas indicate a biogenic origin for the petroleum. $\delta^{13}C$ of −16.2‰ for the bulk inclusion gas suggests a value of −12‰ for the carbonic phase, hence a mix of inorganic CO_2 and organic CO_2 from either thermal alteration of organic matter or in situ chemical oxidation of hydrocarbons. This study has implications for the depth and temperature at which oil may be present, suggesting that deep, old reservoirs may not be completely barren of petroleum. The fact that hydrocarbons in the Matinenda Formation fluoresce indicates that aromatic compounds are able to survive temperatures of up to 350 °C in a suitable geological environment.

Keywords: Fluid inclusions; Oil–CO_2 inclusions; Matinenda Formation; High temperature entrapment; Hydrocarbon metamorphism

1. Introduction

Several types of evidence suggest that oil migration in the early Precambrian was a relatively common phenomenon and may have resulted in high oil saturation being attained in some reservoirs prior to destruction of pore space and structural reactivation of traps (Buick et al., 1998). For example, carbonaceous substances such as kerogen and bitumen are well-documented features of some of the oldest sandstone palaeo-reservoirs in the world and have been the

* Corresponding author. Fax: +61-2-9351-0184.
E-mail address: adriana@es.usyd.edu.au (A. Dutkiewicz).

0009-2541/02/$ - see front matter © 2002 Elsevier Science B.V. All rights reserved.
PII: S0009-2541(02)00271-1

subject of detailed petrographic, isotopic and molecular analyses (e.g. Cortial et al., 1990; Mossman et al., 1993a,b, 2001; George et al., 1994; Parnell, 1996; Buick et al., 1998; Spangenberg and Frimmel, 2001). Other relicts diagnostic of petroleum migration are oil-bearing fluid inclusions which can be preserved as closed systems within their mineral hosts for billions of years (Dutkiewicz et al., 1998). These can also provide important information about fluid composition, migration timing and entrapment conditions which cannot be deduced from solid residues. While oil-bearing fluid inclusions are well-documented in Phanerozoic reservoirs (e.g. Munz, 2001) and have been recorded in late Precambrian rocks (Kvenvolden and Roedder, 1971; Kelly and Nishioka, 1985), few have been described that were trapped prior to 1.1 billion years ago. In this paper we present more complete data on oil-bearing inclusions from the Palaeoproterozoic Matinenda Formation at Elliot Lake, Canada, that were briefly described by Dutkiewicz et al. (1998). One unusual feature of the fluid inclusions is the co-existence of CO_2, oil and water within single, negative crystal-shaped inclusions with trapping temperatures exceeding 250 °C. In this paper, we examine the entrapment conditions and thermal history of these and other types of oil-bearing inclusions in the Matinenda Formation and discuss the implications for survival of complex hydrocarbons at metamorphic temperatures.

2. The Matinenda Formation

The Matinenda Formation at Elliot Lake in Ontario, Canada (Fig. 1) is the ~2.45 billion-year-old locally basal unit of the 10-km-thick Huronian Supergroup (Krogh et al., 1984) (Figs. 1 and 2) and is famous for hosting one of the world's most significant placer uranium deposits (Fralick and Miall, 1989; Dahlkamp, 1993). It comprises several megacycles of a fluvial, fining upwards sequence of feldspathic sandstone and pyritic quartz–pebble conglomerate (Fralick and Miall, 1989). Possible sources of hydrocarbons include mudstones and siltstones of the overlying deltaic McKim and Pecors formations higher in the Supergroup. However, very little is known about these formations in terms of their petroleum generative potential. McKirdy and Imbus (1992) suggested that the black shale of the McKim Formation may have acted as a source rock and seal to the Matinenda Formation reservoir.

The Huronian Supergroup was intruded by mafic sills and dykes of the Nipissing Diabase around 2.2 Ga (Krogh et al., 1984). The main phase of deforma-

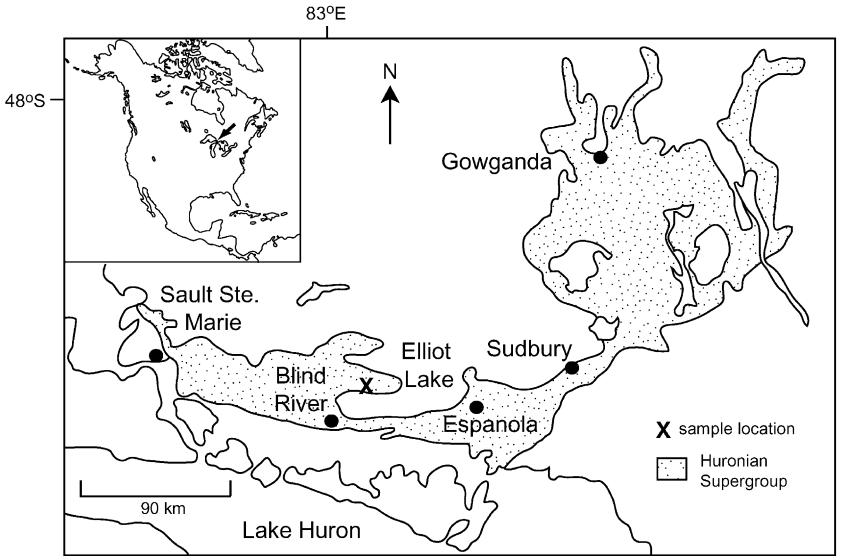

Fig. 1. Sample location map and geographic extent of the Huronian Supergroup. Modified after Mossman (1987).

tion occurred during the Penokean orogeny between ~1.89 and 1.8 Ga, which caused penetrative deformation of the Huronian Supergroup (Young et al., 2001); however, the sequence is only weakly deformed in the study area such that palaeocurrent studies and lithofacies classification are still possible (Fralick and Miall, 1989). Metamorphism in the Supergroup ranges from sub-greenschist to amphibolite facies. The maximum metamorphic grade in the Elliot Lake region never exceeded subgreenschist facies (~200–350 °C) (Willingham et al., 1985) and may have occurred either with intrusion of the Nipissing Diabase (Mossman et al., 1993b) or during the Penokean orogeny (Card, 1978). Partial resetting of isotope systems occurred at about 1.7 and 1.5 Ga subsequent to the Penokean orogeny and these events may represent minor thermal episodes (Hu et al., 1998; McLennan et al., 2000). Although the tectonic setting for the Huronian Basin is still contentious, Fralick and Miall (1989) and Young and Nesbitt (1985) suggested that it was a fault-bounded rifted passive margin that experienced collisional orogeny.

The thickness of the Matinenda Formation in the Elliot Lake area is 180 m (Robertson, 1981) although it reaches up to 600 m elsewhere in the basin (Fralick and Miall, 1989). Locally, it is unconformable over Archaean basement but in other places it conformably overlies mafic volcanic flows and volcaniclastic sediments and underlies the McKim Formation siltstones, mudstones and sandstones (Fralick and Miall, 1989). North of Elliot Lake the Matinenda Formation is unconformably overlain by Ramsay Lake Formation diamictite, which in turn is overlain by the siltstone–mudstone units of the Pecors Formation sandstones (Fralick and Miall, 1989; Fig. 2).

The petrography of the Matinenda Formation has been studied by Robinson and Spooner (1984) and Sutton and Maynard (1993). It comprises coarse-grained, predominantly clast-supported feldspathic quartz arenites and quartz pebble conglomerates derived from Archaean granitic and pegmatitic rocks (Sutton and Maynard, 1993; Vennemann et al., 1995). The framework clasts are well-rounded and range from 0.2 mm to 1 cm in diameter, of which the sand-sized grains tend towards slightly more angular morphologies. Secondary quartz, sericite, feldspar fragments and heavy minerals, especially pyrite, comprise the bulk of the matrix.

The SEM-CL signal from large portions of the sandstone is extremely weak, only faintly showing microfracturing patterns (Fig. 3A). In general, the quartz grains appear zoned with a rim showing a large luminosity contrast (Fig. 3B), possibly related to uranium remobilisation, and rare syntaxial quartz overgrowths (Figs. 3B and 5E–F). Similarly, some microfractures have bright alteration haloes caused by the incorporation of a REE-oxide or carbonate (Rasmussen, pers. comm., 2001). Pressure solution is extensive and has resulted in welding of quartz grains and clasts, reducing porosity effectively to zero. The presence of sericite along grain boundaries, in fracture-fillings within quartz clasts and as intergrowths with secondary quartz led Robinson and Spooner (1984) to conclude that the mineral is a post-depositional alteration product of detrital K-feldspar and was present prior to compaction. Sericite experienced additional growth during compaction. Robinson and Spooner (1984) observed elongate fringes of quartz cement in pyrite pressure shadows and suggest that the bulk of the pyrite is also post-depositional, with only a minor amount of detrital origin.

Sutton and Maynard (1993) identified the following minor mineral phases in the Matinenda Formation: zircon, uraninite, thorite, monazite, xenotime, anatase, magnetite, ilmenite, apatite, bastnaesite, allanite and barite, in addition to which galena, pyrrhotite, chalcopyrite, U–Th silicates (uranothorite and coffinite) and uranous titanates (brannerite) are also present in our samples. The radioactive minerals are of particular interest as they are intimately associated with carbonaceous residues (Willingham et al., 1985; Mossman et al., 1993a,b; Buick et al., 1998). Most workers (Roscoe, 1969; Theis, 1979; Robinson and Spooner, 1984) consider the uraninite to be detrital, derived from pegmatites, and the U–Th silicates and brannerite to be early diagenetic replacement phases after uraninite and ilmeno-magnetite grains. Organic matter in the form of stratiform and globular thucolite has been found at the base of the Matinenda Formation in association with the palaeo-placer deposits (Willingham et al., 1985; Mossman, 1987; Mossman et al., 1993a) and will be discussed in more detail in this paper.

We have studied four samples of the Matinenda Formation. Two are from the Kerr–McGee hole #156-1 from depth intervals 5427′6″–5428′4″ and 5239′0″–5239′6″ and two from an outcrop in the western part of

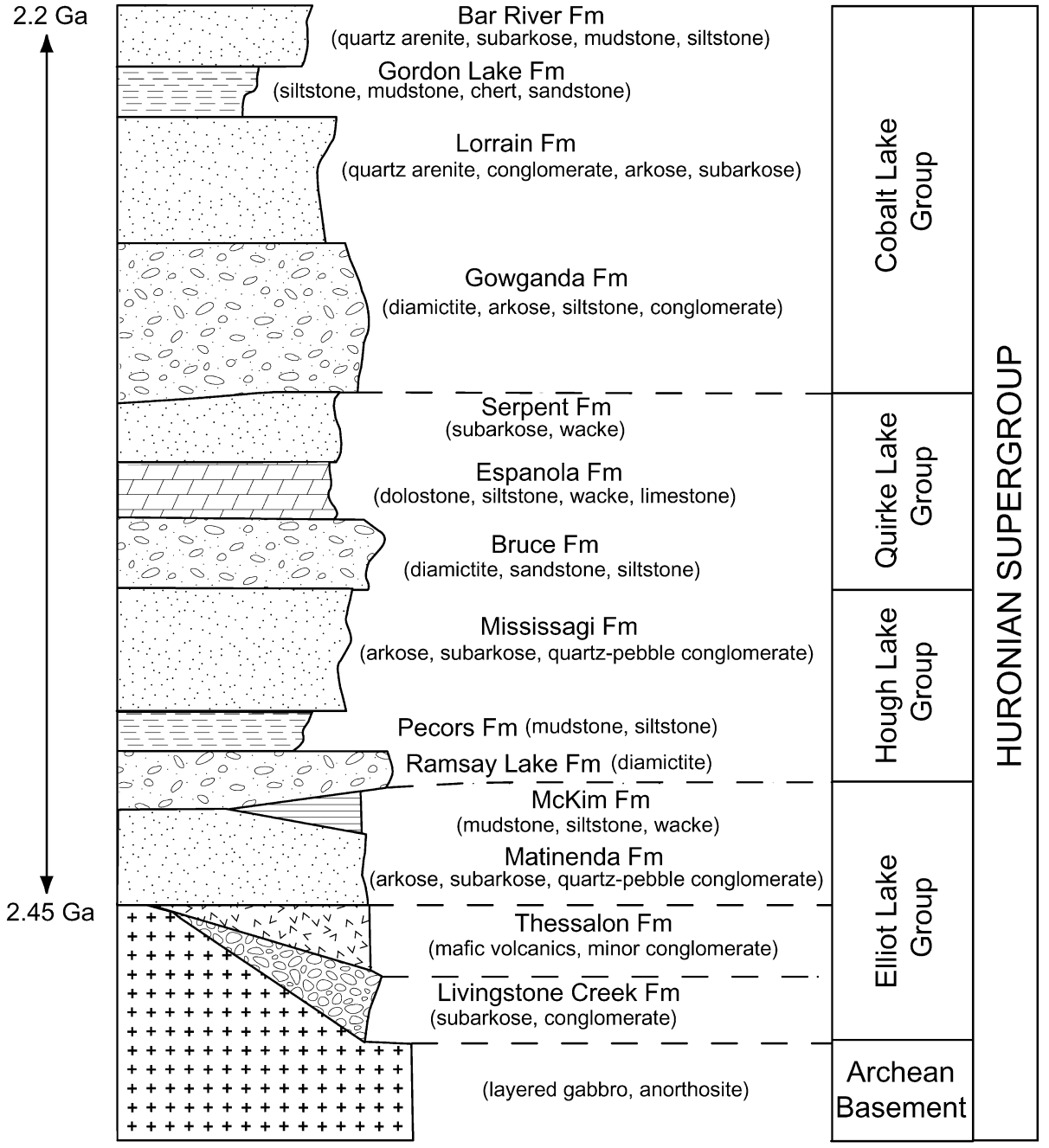

Fig. 2. Stratigraphy of the Huronian Supergroup. Modified after Young (1981).

the Elliot Lake township (corner of Spine Road and Lawrence Avenue). The core samples are from a mineralised zone containing disseminated pyrite and thucolite and comprise a coarse-grained, poorly sorted and poorly bedded feldspathic quartz arenite containing rounded pebbles of quartz up to 1 cm in diameter.

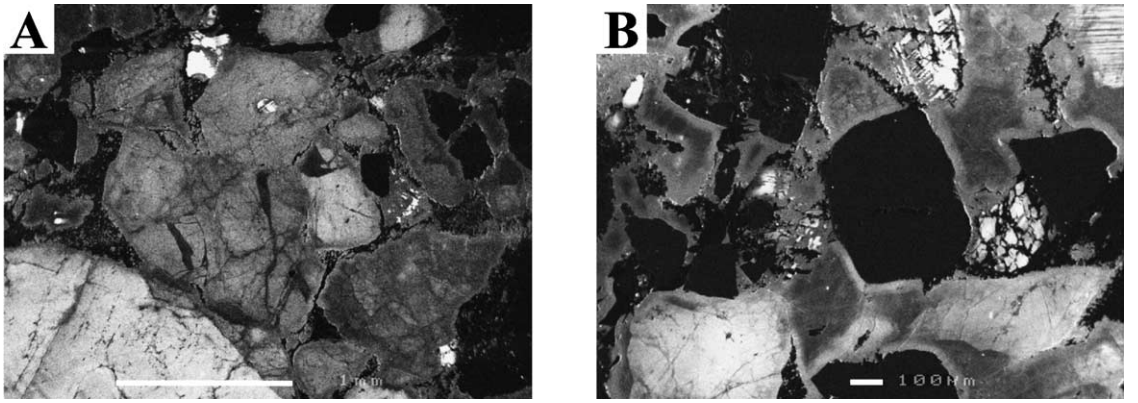

Fig. 3. SEM-CL images of arenites of the Matinenda Formation. The light grey CL rims around the pyrite and quartz grains are probably due to radiation damage of by uranium-bearing fluids derived from partly etched uraninite grains in heavy mineral seams. The partly etched nature of pyrite grains may indicate that the hydrothermal fluid was partly oxidised and carrying dissolved uranium (Rasmussen, pers. comm., 2001). (A) Quartz grains, pyrite (black, non-luminescent) and K-feldspar (white) at the edge of a quartz pebble (light grey, lower left). The sandstone matrix is composed of sericite (black). Non-luminescent regions within detrital quartz grain are intragranular fractures. The fractures lack metamorphic matrix minerals suggesting that cementation did not coincide with metamorphism and post-depositional U-remobilisation. The quartz fracture cement is overprinted by radiation damage rims around quartz grains (central grain, lower right) suggesting that fracturing preceded hydrothermal uranium remobilisation. (B) Pyrite (black, non-luminescent), quartz (medium grey to white), and rare K-feldspar (white) grains in a matrix (black) of sericite with minor chlorite. A possible authigenic quartz overgrowth (dark grey) is discernable around a coarse detrital grain (lower left). Boundaries between detrital quartz grains and between detrital and authigenic quartz are obscured in part by grain–grain pressure solution, grain fracturing, metamorphic reactions involving quartz, and overprinting of original quartz CL signals by radiation damage.

The outcrop samples were taken directly above and below a mineralised zone and consist of moderately sorted medium-grained feldspathic sandstone with 5% by volume of rounded quartz pebbles 1 cm in diameter and several 1-mm-thick heavy mineral partings containing 0.5 mm sub-rounded pyrite and 0.5 mm pyrobitumen nodules. The sandstone is cross-cut by 1-mm-thick chamosite veins with a central pyrite zone. All of the samples contain pyrobitumen nodules and fluorescing oil-bearing fluid inclusions, which are the focus of this study.

3. Analytical techniques

Fifteen doubly polished thick sections were examined. With the exception of pyrobitumen nodule and fluid inclusion petrography, most of the analytical work was carried out on the outcrop samples from Elliot Lake township as these provided ample material for replicate thick sections and for isotope analysis as well as abundant hydrocarbon-bearing fluid inclusions suitable for measurement.

Petrographic study used an Olympus BX60 optical microscope, with a reflected light attachment, UV-epifluorescence and transmitted light. Oil inclusions are most easily recognised by their fluorescence under ultraviolet (UV) light at 365 nm excitation wavelength (Burruss, 1981; Munz, 2001). Maximum total magnification of the inclusions was 1000 ×. UV and transmitted light and their respective diaphragms were used to confirm the presence of liquids and solids within the inclusion cavities. Particular care was taken to distinguish artefacts caused by scattering of light from genuine oil-bearing fluid inclusions (Burruss, 1991). Images were captured using a Nikon E800 microscope equipped with a Sensicam digital camera. A Philips SEM 505 equipped with backscattered electron-dispersive spectroscopy (EDS) allowed elemental analysis of individual mineral phases at a 10 μm scale. Back-scattered electron (BSE) microscopy and cathodoluminescence (SEM-CL) was carried out on petroliferous sandstones and conglomerates to identify mineral components and to establish the relative timing of fluid inclusion entrapment. The SEM work was done with a JEOL 6400 Scanning

Microscope, using a beam current of 3 nA and an accelerating voltage of 15 kV.

The microthermometric analysis was carried out using a Linkam system equipped with a THMS 600 heating–freezing stage, an LNP cooling system and a TMS94 temperature controller. The stage was calibrated using synthetic H_2O and CO_2 fluid inclusions obtained from Fluid Inclusions of Texas. Precision is estimated to be ± 0.2 °C for cooling runs and ± 2 °C for the homogenisation temperatures. Phase transitions of approximately 250 quartz-hosted inclusions were measured.

Laser Raman spectroscopic analysis of most phases in about 35 individual fluid inclusions was performed at Geoscience Australia in Canberra on a Dilor Super-Labram spectrometer. The spectrometer was equipped with a holographic notch filter, 600 and 1800 g/mm gratings, and a 2000×450 pixel CCD detector. The inclusions were illuminated with 514.5 nm laser excitation from a Spectral Physics model 2017 argon ion laser, using 5 mW power at sample level, and a single 10, 15 or 30 s accumulation. A 100 × Olympus microscope objective was used to focus the laser beam on separate inclusion phases and collect the scattered light. The focused laser spot on the samples was approximately 1 μm in diameter. As laser-induced fluorescence of oil interferes with the Raman signal, only weakly fluorescing and non-fluorescing inclusions were chosen for this analysis.

Carbon isotope analysis was performed on pyrobitumen nodules and on fluid inclusion gases using an Elemental Analyser-Isotope Ratio Mass Spectrometry (EA-IRMS) system at CSIRO in Sydney. The purpose of the ^{13}C analysis of the inclusions was primarily to provide insights into the origin of CO_2 and the relationships between hydrocarbon phases. The nodules were isolated by crushing 100 g of the sample, digesting it in HF acid and separating out the heavy minerals using heavy liquids. For the inclusion gases, the sample was lightly crushed, oxidised for about 5 weeks in hydrogen peroxide and digested in chromic acid for 2 days. This was done to remove any solid organic residues such as bitumen and to separate the quartz grains as much as possible without destroying the fluid inclusions trapped within quartz-hosted microfractures. The isolated quartz grains were subsequently heated overnight at 50 °C to remove surface water. Gas was collected in evacuated glass tubes during gradual thermal decrepitation of the inclusions between 50 and 400 °C for over 2 h. This was deemed sufficient because microthermometric measurements showed that the majority of CO_2-rich inclusions decrepitated around 320 °C. Higher decrepitation temperatures were avoided because of recognised problems involving reactions between inclusion gases (Hoefs and Stalder, 1977). Approximately 200 g of sample was decrepitated in two separate batches. The hydrocarbon gases were collected using a liquid nitrogen trap. The sample was oxidised at 800 °C for 5 h and then analysed for ^{13}C. The CO_2 gas from the fluid inclusions could not be isolated successfully from the hydrocarbon gases because of the conformation of the vacuum distillation line used. Consequently, we only have ^{13}C measurements of low molecular weight hydrocarbon gases and of bulk gas. Analytical precision is ± 0.2‰.

4. Pyrobitumen nodules

Carbonaceous nodules are relatively common within the Matinenda Formation averaging about twelve nodules per standard thin section and are associated with laminae containing radioactive and heavy mineral grains (Fig. 4). The nodules are generally isolated but may occur in small clusters. They are usually between 200 and 400 μm in diameter, have an irregular globular shape and are rarely fractured. Smaller nodules measuring between 10 and 50 μm occur in the surface samples together with the larger nodules. Such nodules were observed previously by Kaiman and Horwood (1976) and Mossman (1987) who recognised their carbonaceous and radioactive nature. In addition to nodules, Mossman (1987) observed 6 mm long irregular streaks of carbonaceous matter within the arenite/conglomerate matrix, which were not present in our samples.

The nodules appear black under transmitted light although a dark brown colour is evident at their margins where the nodules are relatively thin. The nodules are grey under reflected light and mineral inclusions contained within them also display a grey colour, which is distinctly different from that of the carbonaceous material. Due to their mean atomic number, the nodules appear black and the mineral inclusions white or light grey using SEM backscat-

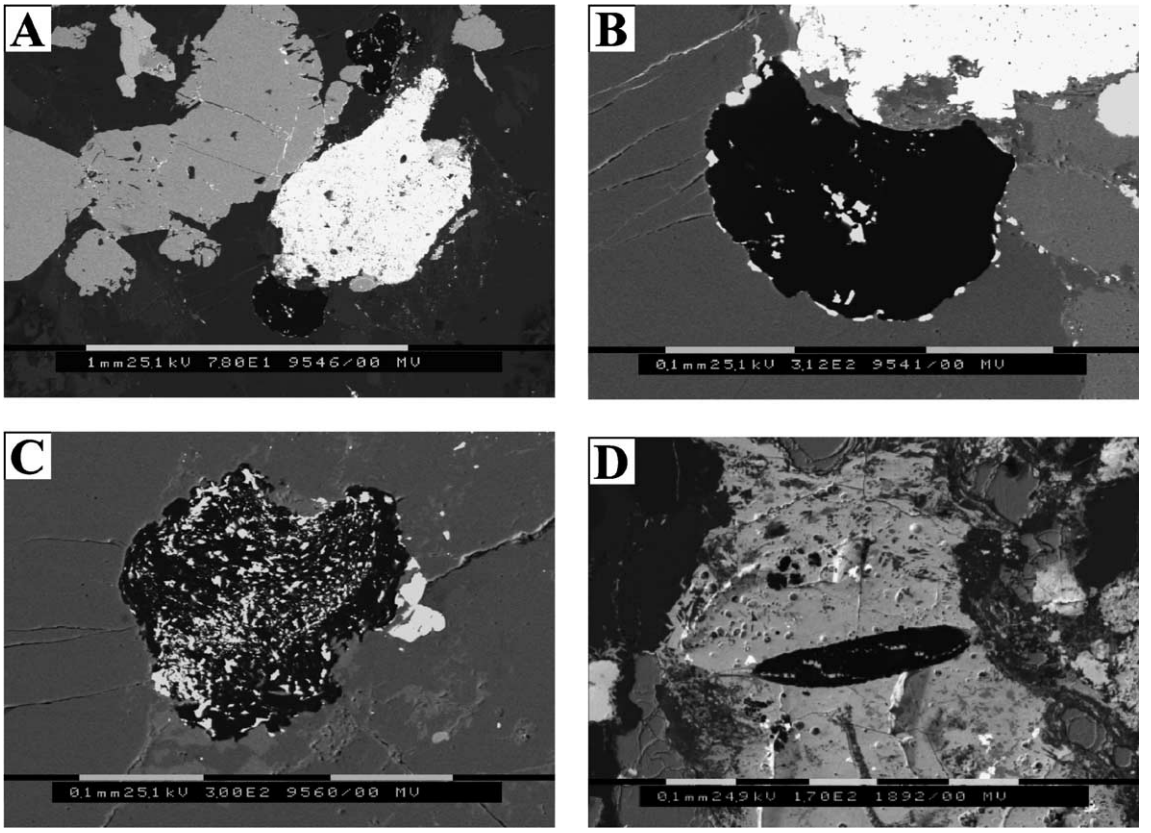

Fig. 4. Backscattered SEM images of bitumen nodules in the Matinenda Formation. (A) Two bitumen nodules (black) containing tiny sulphide inclusions within a heavy mineral band comprising pyrite (grey) and brannerite (white) surrounded by quartz (dark grey). (B) Close-up of (A) showing a droplet-shaped bitumen nodule containing inclusions of pyrite, chalcopyrite, galena and pyrrhotite. Background consists of brannerite (white), K-feldspar (light grey) and quartz (dark grey). (C) Bitumen nodule containing wispy and blocky inclusions of uranothorite and thorian coffinite. Minor inclusions of galena and muscovite also present. The nodule is enclosed by quartz (dark grey), K-feldspar (light grey) and pyrite (white). (D) Elongate bitumen nodule containing inclusions of bastnaesite and galena. Smaller, spherical and inclusion-free nodules containing trace amounts of uranium also present. Nodules are surrounded by needle-like brannerite (light grey). Other minerals include quartz (very dark grey), K-feldspar (dark grey), pyrrhotite (medium grey), uranothorite (light grey; middle left) and muscovite (dark grey inclusions within brannerite).

tered imaging. Based on their morphology and composition and by analogy with Phanerozoic and Precambrian counterparts (Rasmussen, 1997; Buick et al., 1998) we interpret the nodules to be radiogenic pyrobitumen formed when fluid hydrocarbons were immobilised by polymerisation under α-particle bombardment.

EDS analysis indicates that the pyrobitumen is chiefly composed of carbon with minor sulphur and oxygen while the mineral inclusions are dominated by sulphides and radioactive uranium–thorium minerals. Small bitumen nodules in Fig. 4D contain U with no visible solid inclusions. The non-radioactive minerals are pyrite, galena, pyrrhotite, chalcopyrite, phyllosilicates and bastnaesite (Ce, La, $Y(CO_3)F$) (Fig. 4). The most common radioactive minerals within the nodules are U–Th silicates which are blocky, wispy or elongate and fall into two groups depending on their relative U and Th abundances. The first consists predominantly of U and Si with moderate to minor amounts of Th, Pb, Y, Fe and Ca. The second group is dominated by Th and Si with U in moderate to high abundance and minor Pb, P,

Ca and Fe. The compositions are consistent with thorian coffinite ($U(SiO_4)_{1-x}(OH)_4$) and uranothorite ($(Th>U)SiO_4$) which are known to be present at Elliot Lake (Robertson, 1981). Uraninite is a relatively minor component of the pyrobitumen nodules and is dominated by U and Pb with minor Th, Si, Al, Y, Ca and Fe. Also present are uranous titanates containing Ti, U, Si, Fe, Y, Pb, S, Al and minor Ce and Th, which are consistent with brannerite ($(U, Ca, Ce)(Ti,Fe)_2O_6$) composition. The brannerite inclusions are either prismatic or blocky and although intimately associated with the pyrobitumen nodules, only rarely occur within them (Fig. 4A,B).

5. Fluid inclusions

Fluid inclusions are extremely abundant within our samples of the Matinenda Formation and are located within microfractures in quartz and K-feldspar grains and within rare quartz overgrowths. Trails with complex cross-cutting relations and irregular clusters are common. Most inclusions are aqueous, 2 to 20 μm in size and are variably spherical, irregular or nearly negative crystal-shaped. Gas bubbles comprising 10 to 40% of the inclusion volume are common and are occasionally mobile at room temperature. A highly birefringent solid (most probably either calcite or nahcolite) is present within some inclusions. Gas-rich inclusions, consisting of 30 to 95 vol.% gas, also occur as apparently separate assemblages within fracture trails and clusters and as isolated individuals. These are on average larger than the aqueous inclusions, measuring between 10 and 20 μm, and most commonly occur within quartz clasts.

About 30% of the total fluid inclusion population is oil-bearing and displays bright blue, cream, yellow and orange fluorescence under ultraviolet excitation. Yellow, orange and yellow-cream inclusions are most abundant. In general, the inclusions are 2 to 20 μm long (usually 2 to 5 μm and rarely up to 50 μm long) and display morphologies ranging from highly irregular to negative crystals. At the 2 μm scale, the inclusions are too small for the recognition of discrete fluid phases although some appear to have dark centres which likely represent tiny gas bubbles. The majority of the minute inclusions display orange fluorescence and are restricted to the most deformed parts of clasts. The larger inclusions are located within micro-fractures cutting detrital quartz and feldspar grains, which also host coeval non-fluorescent inclusions of similar composition but without the hydrocarbon phase (Fig. 5). Many of the inclusions occur in dense clusters within original detrital grains and cannot be assigned to a particular micro-fracture. Occasionally, these grains are cross-cut by fractures containing iron oxide minerals but lacking fluid inclusions (Fig. 5A–B) or surrounded by recrystallised quartz also lacking oil-bearing fluid inclusions (Fig. 5C–D,G–H). However, fluorescent aqueous inclusions are present within the rare syntaxial quartz overgrowths (Fig. 5E–F). None of the microfractures hosting oil-bearing fluid inclusions was observed to cut across present-day grain boundaries. In addition, there is no discernable time relationship between different types of inclusions (discussed below). However, water-rich and gas-rich inclusions occur in separate fracture trails or clusters within the same grain or clast (Fig. 5).

Inclusions located in the least deformed parts of the quartz grains and lacking decrepitation haloes were selected for examination and thermometric analysis. Their composition is diverse and complex, with large variations both between and within fluid inclusion assemblages. Individual inclusions have up to four fluid phases and two solid phases. We distinguish four oil-bearing types of fluid inclusions based on broad compositional parameters as determined by a combi-

Fig. 5. Photomicrographs of fluid inclusion textures. A, C, E, G: UV-epifluorescence; B, D, F, H: transmitted light, crossed-nicols. (A–B) Predominantly CO_2-dominated fluorescing oil-bearing inclusions within microfractures cut by a later fractures containing iron oxide minerals. The inclusions are present within a relatively undeformed quartz grain and display a range of fluorescence colours. (C–D) A relatively large detrital quartz grain containing abundant fluorescing fluid inclusions. The grain is surrounded by recrystallised quartz which lacks fluorescing fluid inclusions. (E–F) Tiny, orange-fluorescing oil-bearing fluid inclusions decorating an outer, inclusion-rich quartz overgrowth around an otherwise inclusion-barren quartz grain. The matrix consists of very fine-grained quartz. (G–H) Fluorescing, oil-bearing H_2O inclusions in the inner core of a quartz grain within microfractures that terminate at the core–overgrowth boundary. The outer rim of the quartz grain is virtually inclusion-free. Non-fluorescent fluid inclusions occur along the crystal boundaries.

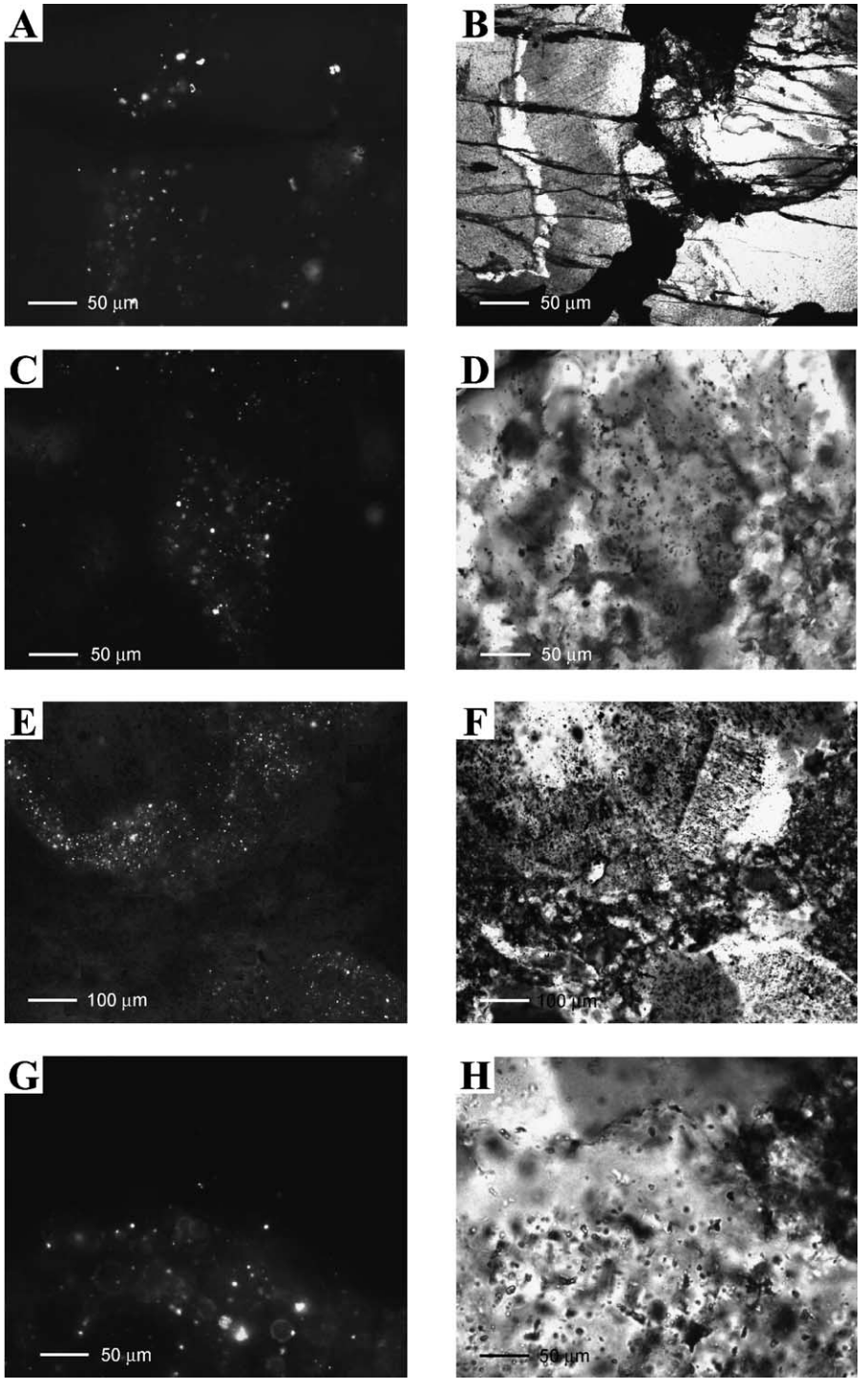
A
50 μm
B
50 μm
C
50 μm
D
50 μm
E
100 μm
F
100 μm
G
50 μm
H
50 μm

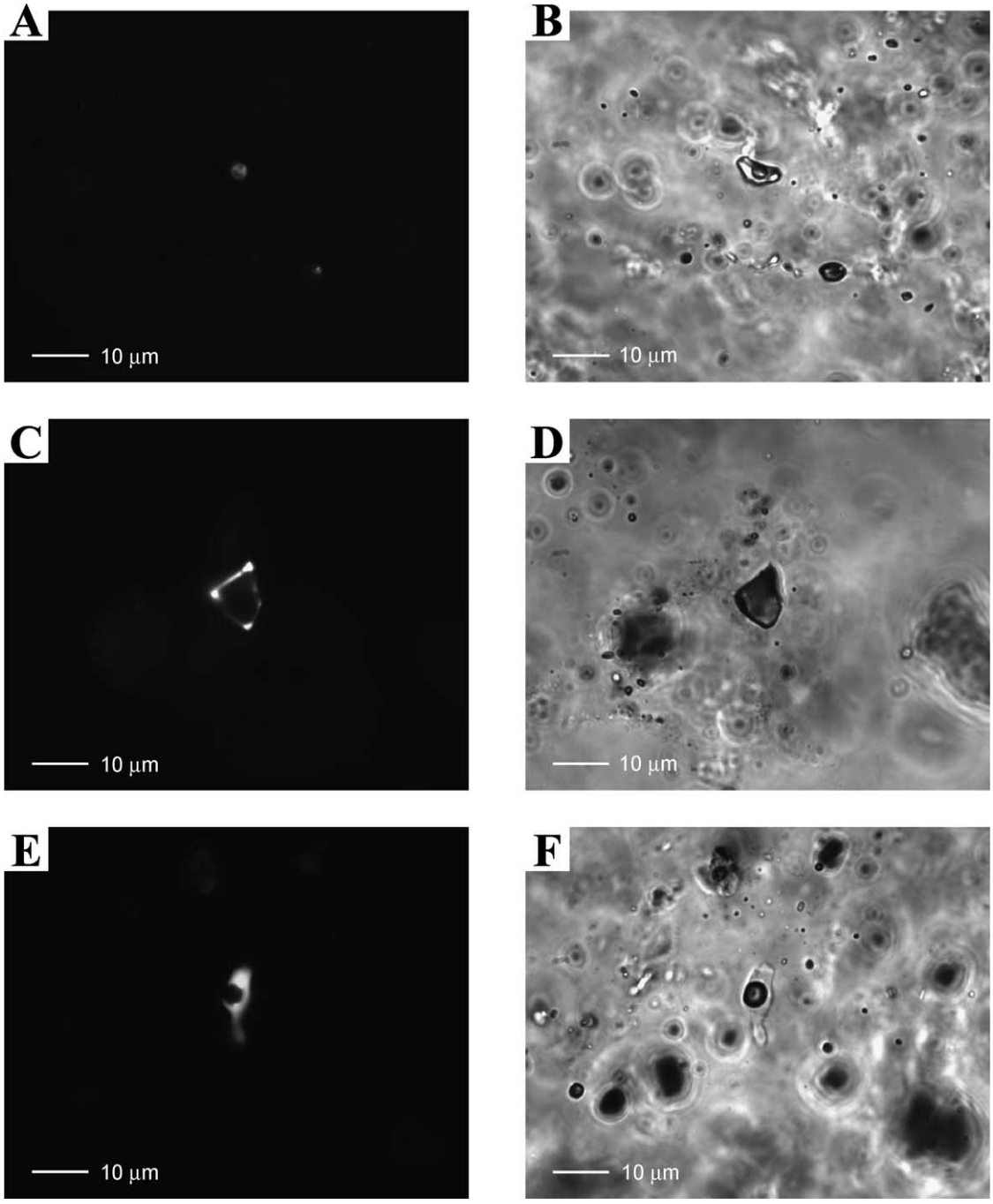

Fig. 6. Photomicrographs of oil-bearing inclusion types at room temperature. A, C, E: UV-epifluorescence; B, D, F: transmitted light, crossed-nicols. (A–B) Type 1 inclusion comprising a high salinity aqueous phase and oil. The oil forms a cream fluorescing rim around the gas bubble. (C–D) Type 3 inclusion comprising light hydrocarbon and oil with water and a solid. The oil forms a thin fluorescing rim around the hydrocarbon gas bubble. (E–F) Type 4 inclusion comprising oil and gas. The oil fluoresces blue.

nation of petrography (Figs. 6 and 7), microthermometry and laser Raman spectroscopy:

- Type 1: Inclusions dominated by water, with or without a minor oil phase, a solid (calcite and/or rarely bitumen?), and with detectable methane;
- Type 2: Inclusions with a significant to volumetrically dominant carbonic phase, together with variable combinations of a minor oil phase, an aqueous phase, light hydrocarbons, and solid phases;
- Type 3: Inclusions dominated by a light hydrocarbon gas phase, with variable combinations of a minor oil phase, an aqueous phase, and a solid (bitumen), but no detectable CO_2;
- Type 4: Inclusions dominated by oil and gas.

Types 1 and 2 inclusions are by far the most common types in the Matinenda Formation and were studied in most detail. Type 4 inclusions are rare (Figs. 6 and 7). In the following sections, microthermometric data are presented for Types 1 and 2 inclusions, in all cases distinguishing between those with and without oil. A small number of inclusions had not fully homogenised at 400 °C. However, it was decided not to heat them further in order to preserve inclusions for future study. Such inclusions formed a minority of any assemblage and high homogenisation temperatures are thus not representative.

5.1. Type 1 inclusions: aqueous-oil

Type 1 inclusions are on average about 6–10 μm long but may be up to 30 μm in length and are ellipsoidal, near-spherical or highly irregular in shape. In many cases, coeval aqueous and H_2O-oil inclusions occur along a single fracture surface. The inclusions typically consist of 80 to 85% liquid water, a water-dominated vapour phase which occupies 12% to 16% of volume, and oil forming 2% to 5% of volume. The oil is evenly distributed as a film on the surface of the gas bubble (Fig. 6A–B), forms a crescent-shaped partial rim around the gas bubble or occurs as micron-sized globules within the aqueous phase. Occasional solids include calcite and a brownish organic phase (bitumen?) identified using laser Raman analysis. Gas bubbles are frequently mobile and the oil phase is always colourless in transmitted light. Although difficult to analyse due to strong fluorescence around a relatively small gas bubble, laser Raman analysis of the gaseous phase indicates that the majority of inclusions are dominated by water vapour which in some instances is accompanied by a small amount of dissolved CH_4. CO_2 was not detected in any of these inclusions. However, only a dozen inclusions were measured due to problems associated with fluorescence, mobile vapour bubbles and bubble size, so the possible presence of CO_2 and other gases cannot be excluded completely. Clathrate formation was not observed although several inclusions displayed metastable ice-melting behaviour.

Melting temperatures of ice in both aqueous and oil–water inclusions show a bimodal distribution (Fig. 8) with the main mode between −18 and −28 °C and the lesser mode between −0.8 and −6 °C. Eutectic temperature was difficult to determine due to the small size of the inclusions and metastability. However, a small number of inclusions contain a solid calcite crystal, which in one inclusion melted at 225 °C. Many inclusions were found to stretch and leak at these temperatures so that melting temperatures of daughter crystals could not be determined. Some of the most saline inclusions show definite crystals below −40 °C following warming of the supercooled fluids indicating $NaCl–CaCl_2–H_2O$ composition (Goldstein and Reynolds, 1994). Consequently, the main mode of the melting temperatures of ice for coeval aqueous and oil-bearing fluid inclusions corresponds to a range of 20 to 25 wt.% NaCl equivalent using the relationships presented in Goldstein and Reynolds (1994) and Oakes et al. (1990). Using the methodology of Mernagh and Wilde (1989), laser Raman analysis of the aqueous phase confirms the high salinity of the inclusions (Fig. 9). No eutectic melting or inclusion "clearing" was observed for the smaller population with higher ice melting temperatures. Most of these inclusions, however, freeze around −43 °C, which is above the eutectic temperature for the $NaCl–CaCl_2–H_2O$ system. For these inclusions a $H_2O–NaCl$ model composition is assumed (Bodnar, 1993) yielding salinities of 1.4 to 9.1 wt.% NaCl equivalent.

For the majority of inclusions, homogenisation of liquid and vapour to liquid took place between 80 and 220 °C (Fig. 10). The main mode for aqueous inclusions (90 to 120 °C) is slightly lower than for oil-bearing ones (120 to 140 °C). A small number of

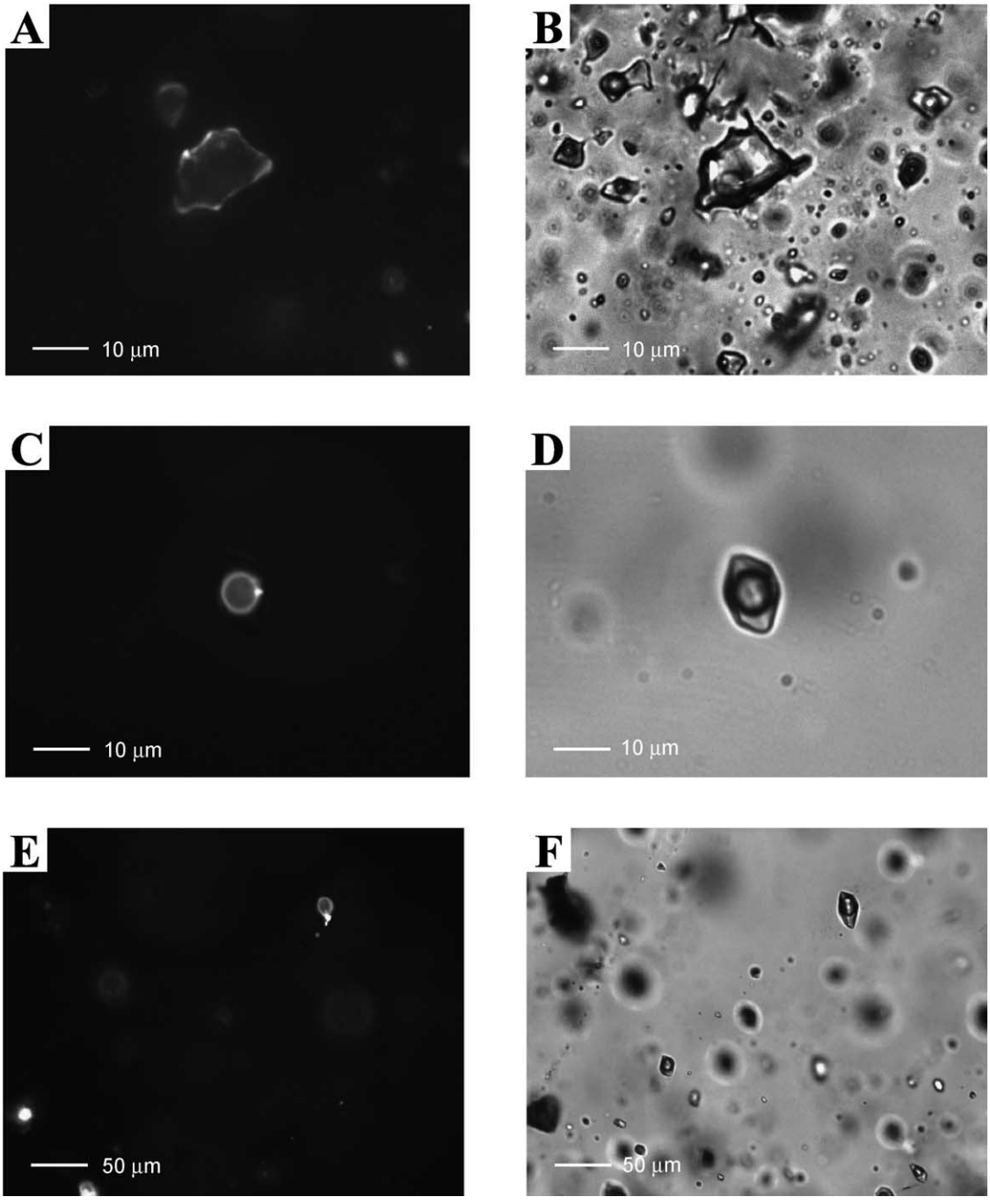

Fig. 7. Photomicrographs of Type 2 mixed carbonic–aqueous inclusions with oil. A, C, E: UV-epifluorescence; B, D, F: transmitted light, crossed-nicols. (A–B) Irregularly shaped inclusion with oil forming a cream-fluorescing rim at the interface between the aqueous and carbonic phases. Note the double bubble in the carbonic fluid. (C–D) Typical negative crystal shape of the mixed carbonic–aqueous-oil inclusions. Oil forms a thin cream-fluorescing rim around the carbonic fluid. (E–F) Mixed fluorescent and non-fluorescent Type 2 inclusions within a microfracture in a quartz clast. Fluorescence colour ranges from orange to cream and blue.

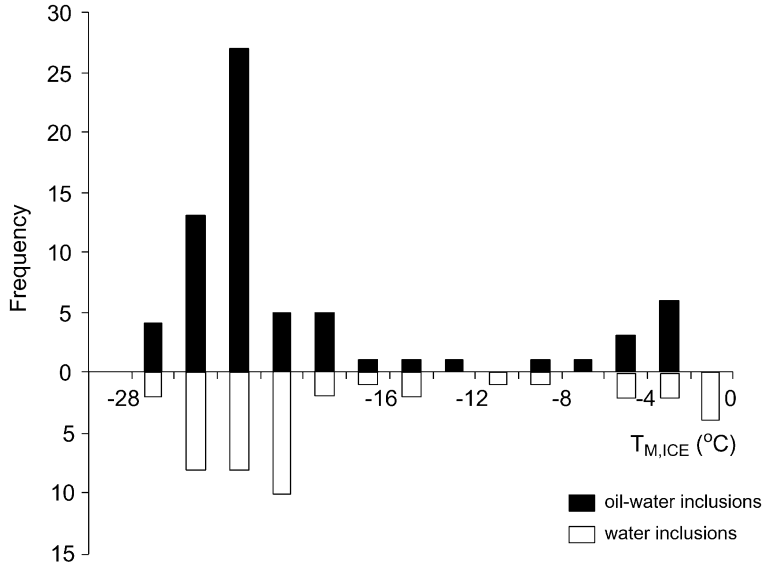

Fig. 8. Ice-melting temperatures ($T_{M,ICE}$) for Type 1 aqueous-oil inclusions divided into oil-bearing and aqueous only inclusions.

Type 1 inclusions homogenised to liquid at significantly higher temperatures (230 to 370 °C). Cycling of homogenisation temperatures of the oil-bearing inclusions was very difficult and in most cases the recorded temperature represents the last temperature at which the bubble was clearly visible. There was no rapid return of the gas bubble on cooling even when the inclusion was heated 50 °C above apparent homogenisation, but rather a gradual growth. As this behaviour was not observed in the aqueous inclusions,

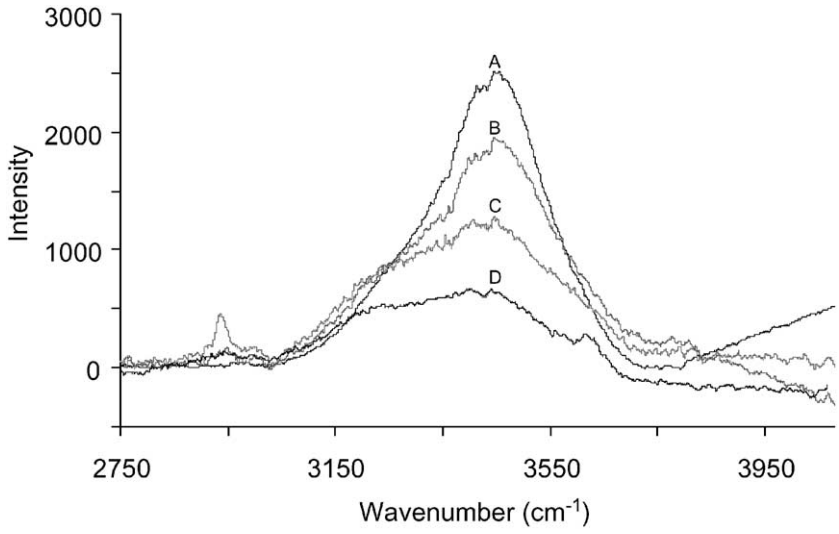

Fig. 9. Raman spectra of the aqueous phase associated with different inclusion types. (A) Type 1 aqueous-oil inclusion; salinity 26 ± 4 wt.% NaCl. (B) Type 2 mixed carbonic–aqueous with oil inclusion; salinity 17 ± 4 wt.% NaCl. (C) Type 2 mixed carbonic–aqueous with oil inclusion; salinity 6.5 ± 2 wt.% NaCl. (D) Type 3 light hydrocarbon and oil with water inclusion; salinity too low to be determined using the method of Mernagh and Wilde (1989).

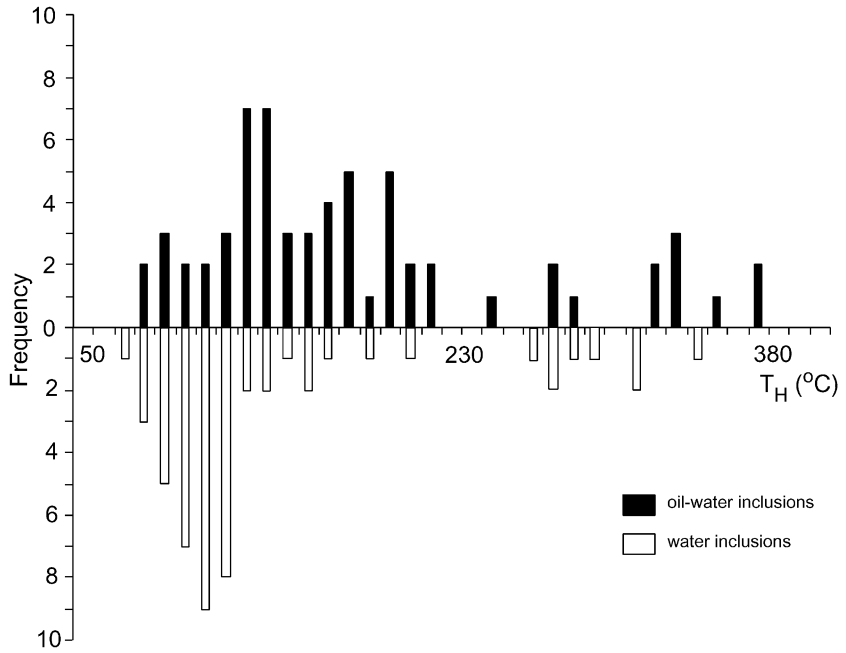

Fig. 10. Total homogenisation temperature ($T_{H\ L+V \rightarrow L}$) for Type I aqueous-oil inclusions divided into oil-bearing and aqueous only inclusions.

we suspect that the presence of oil affects the homogenisation of the liquid water and vapour phases. Homogenisation temperatures greater than 200 °C are interpreted to represent in part inclusions that have stretched or leaked, as indicated by plots of homogenisation temperature versus ice melting temperature and of homogenisation temperature versus bubble length:inclusion length (Figs. 11 and 12). The gas

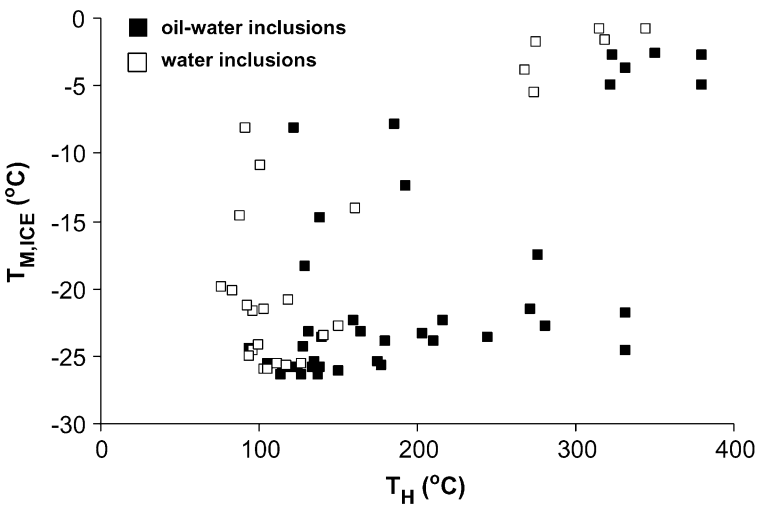

Fig. 11. Total homogenisation (T_H) versus ice-melting temperature ($T_{M,ICE}$) plot for Type 1 aqueous-oil inclusions divided into oil-bearing and aqueous only inclusions.

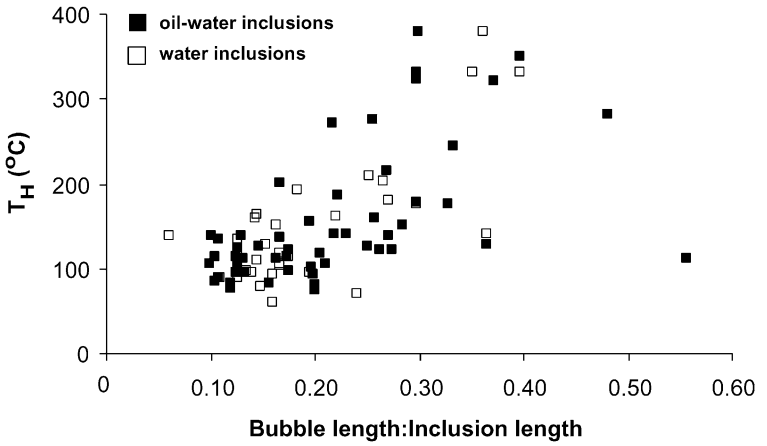

Fig. 12. Total homogenisation temperature (T_H) versus bubble length: inclusion length for Type 1 aqueous-oil inclusions divided into oil-bearing and aqueous only inclusions.

bubble size of some of these inclusions increased following heating to the homogenisation temperature. The subpopulation of inclusions with high homogenisation temperatures and low salinity (Fig. 11) cannot be the result of stretching of another subpopulation and these are thus interpreted to have been trapped at high temperatures. The small number of inclusions which have melting temperatures of ice intermediate between the two modes and low temperatures of homogenisation are interpreted to be the result of mixing of waters with different salinities. Oil is present within all these sub-populations.

5.2. Type 2 inclusions: carbonic phase dominant

Type 2 inclusions have two to four fluid phases at room temperature and up to two solid phases. These inclusions are generally larger than the water–oil inclusions, up to 25 μm, with smaller individuals frequently approaching spherical and negative crystal shapes. The aqueous phase forms up to 70% of inclusion volume, but is not visible in some inclusions. The carbonic phase forms between 30% and 97% of inclusion volume, and is composed of either CO_2 liquid with, in some cases, a rapidly moving bubble of CO_2 gas, or a dark gaseous bubble. Oil, where present, occupies 2 to 3 vol.% as a yellow to cream or occasionally blue fluorescing rim to the carbonic phase (Fig. 7). Fluorescing micron-sized globules of oil are also occasionally located at the interface between the carbonic and aqueous fluids. Highly birefringent solid daughter crystals of, most likely, nahcolite or calcite occur in many inclusions in consistent proportions relative to the fluid phases. Unidentified accidental crystals are also present. The inclusions tend to occur in clusters rather than in well-defined microfracture trails. Assemblages of inclusions with negative crystal shapes often have very consistent aqueous to carbonic phase ratios and display consistent fluorescence colours within a particular cluster. Oil-bearing inclusions occur together with mixed aqueous–carbonic subtypes which lack liquid hydrocarbons (Fig. 7E–F).

As fluorescence posed a problem, usually only CO_2 Raman peaks were detected above the high background. In inclusions where the fluorescent oil phase was concentrated in one part or where the gas bubbles were exceptionally large, laser Raman spectroscopy shows that inclusions with visible bubbles at room temperature are dominated by CO_2 with trace amounts of dissolved CH_4 (Fig. 13). Generally, they comprise 95 to 97 mol% CO_2 and 2 to 5 mol% CH_4. In a small number of inclusions, the CH_4 reaches about 50 mol% accompanied by 2 to 8 mol% C_2H_6 and 1 to 5 mol% C_3H_8. Typical Raman traces of the gaseous and aqueous phases are shown in Figs. 9 and 13.

Measured melting temperatures of the carbonic phase range from −70 to −56.6 °C (Fig. 14). The mode for oil-bearing inclusions is slightly lower, and the proportion of such inclusions, which have carbonic phase melting temperatures below −58 °C, is slightly

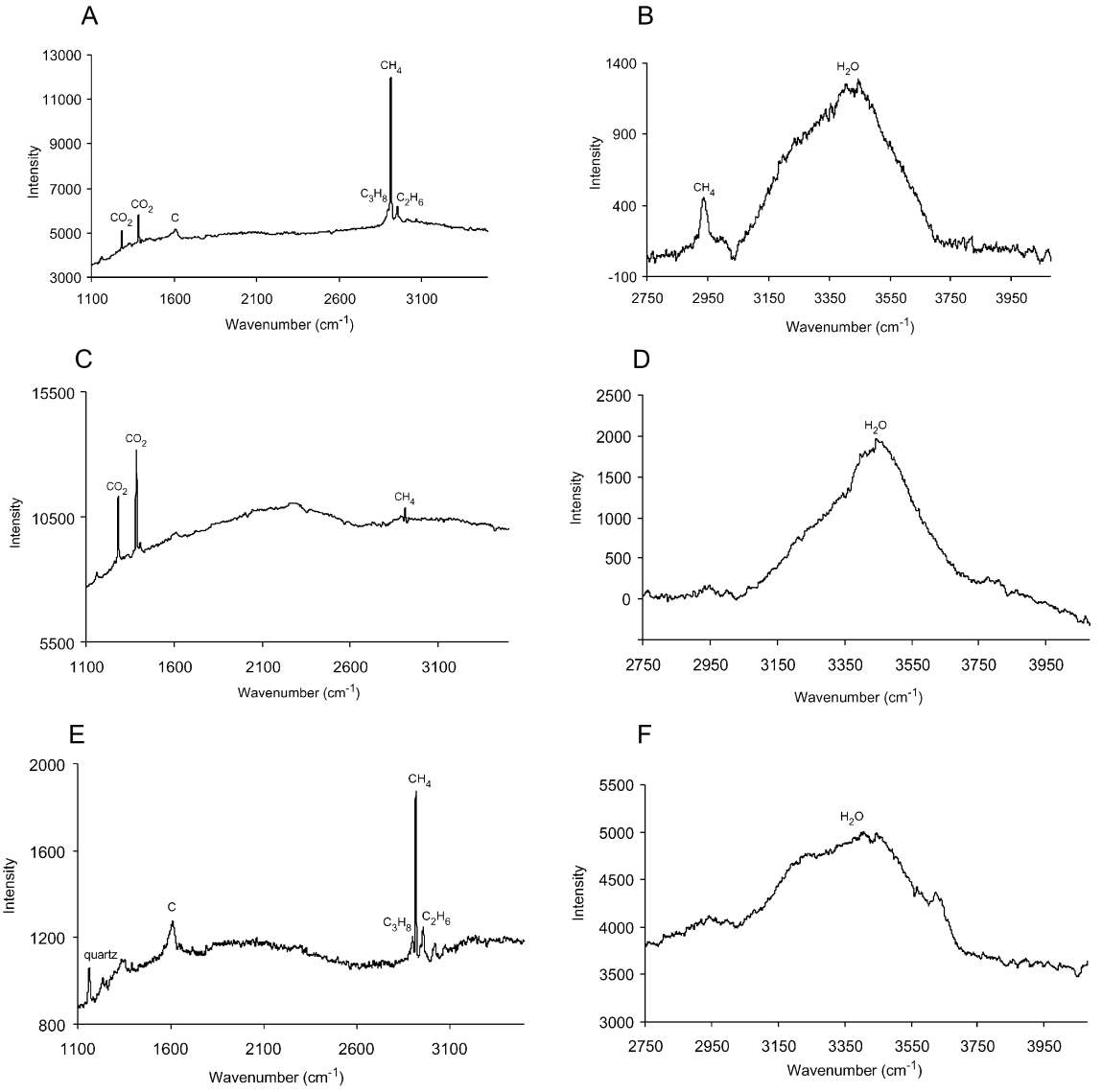

Fig. 13. Raman spectra of gaseous and aqueous phases in different inclusion types. (A–B) Type 2 mixed carbonic–aqueous with oil inclusion with a carbonic phase of 50 mol% CH_4, 2–8 mol% C_2H_6 and 1–5 mol% C_3H_8 and a relatively low salinity (6.5 wt.% NaCl) aqueous phase. (C–D) Type 2 mixed carbonic–aqueous with oil inclusion with 5 mol% CH_4 and 95 mol% CO_2 in the carbonic phase. The aqueous phase has a moderate to high salinity of ~ 17 wt.%. (E–F) Type 3 light hydrocarbon and oil with water inclusion with 91 mol% CH_4, 7 mol% C_2H_6 and 2 mol% C_3H_8 in the hydrocarbon phase. No CO_2 was detected in these inclusion types.

greater. The carbonic phase homogenised to either liquid or vapour over a wide temperature range from −22.9 to 30.9 °C (Fig. 15). The majority of inclusions, however, homogenised above 26 °C. There is no difference in homogenisation of fluorescent and non-fluorescent sub-types. These data are consistent with the Raman spectra: the carbonic phase is in most inclusions dominantly CO_2 with a few percent light hydrocarbons, but a minority of Type 2 inclusions have up to about 50% CH_4.

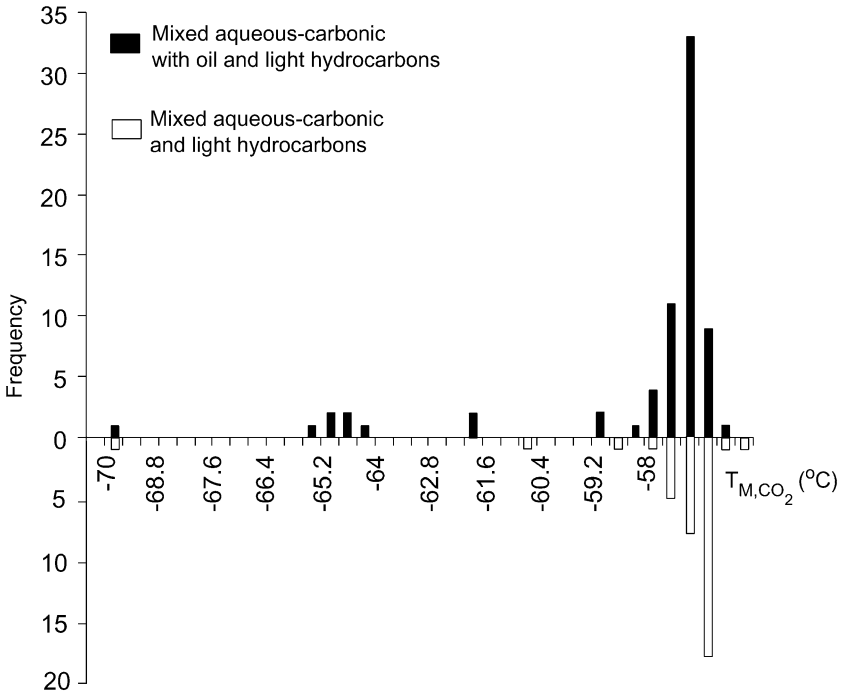

Fig. 14. Carbonic phase melting temperatures ($T_{M,CO_2\ S+L+V\rightarrow L+V}$) for Type 2 mixed aqueous–carbonic inclusions.

Clathrate melting and eutectic temperatures were very difficult to measure for many inclusions owing to the small amount of water. Melting temperatures range from 2.8 to 11.6 °C for the aqueous–carbonic-oil inclusions indicating formation of complex clathrates (Fig. 16). For the aqueous–carbonic inclu-

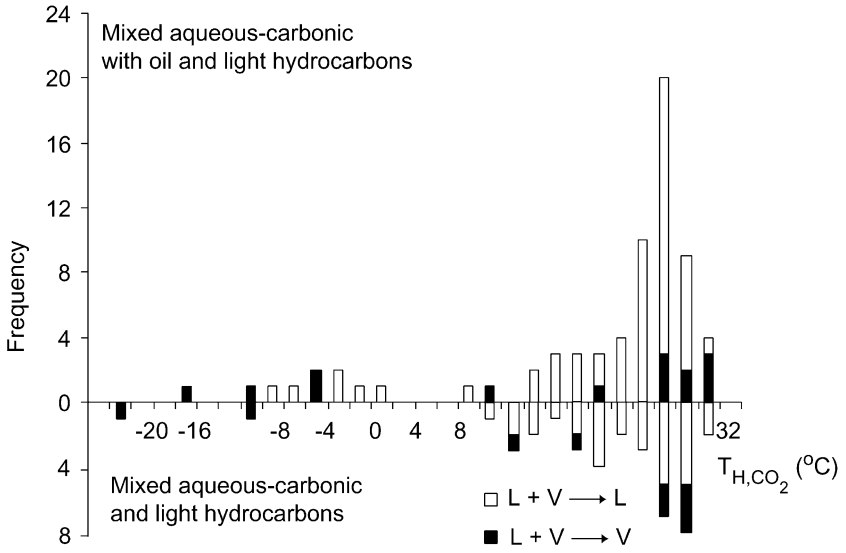

Fig. 15. Homogenisation temperatures of the carbonic phase (T_{H,CO_2}) for Type 2 mixed aqueous–carbonic inclusions.

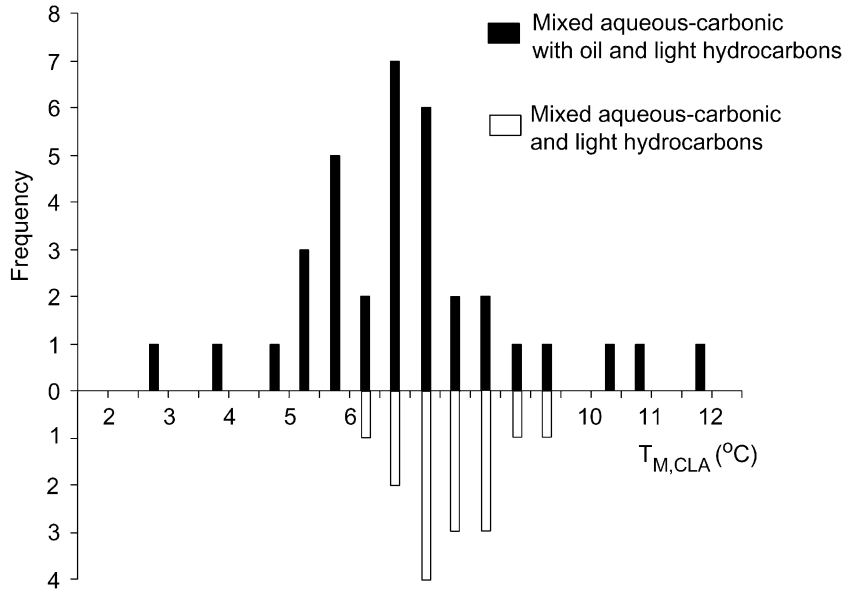

Fig. 16. Melting temperatures of clathrates ($T_{M,CLA}$) for Type 2 mixed aqueous–carbonic inclusions.

sions, clathrate melting occurs in a narrower range from 6.5 to 9.4 °C. Overall, however, the distribution of clathrate melting temperatures is very broad for both inclusion sub-populations. The high temperatures of clathrate melting and freezing of the aqueous phase, just above −40 °C, suggest an NaCl–CO_2–H_2O system and so the relationship presented in Diamond (1992) was used to convert the temperatures to wt.% NaCl. The salinities for aqueous–carbonic-oil inclusions range from 1.8 to 12.1 wt.% NaCl for simple CO_2 clathrate, although laser Raman analysis indicates that salinities as high as 17 wt.% NaCl may occur (Fig. 9). Salinities of the aqueous–carbonic inclusions range from 1.2 to 6.5 wt.% NaCl. Notably, salinities as high as those found in the Type 1 oil–water and aqueous inclusions were not calculated for Type 2 inclusions. Birefringent daughter phases in two inclusions melted at 167 and 177 °C, a temperature suggesting that these are likely nahcolite. Other small daughter phases (calcite?) showed a small reduction in size with increasing temperature but persisted as solids up to 400 °C (the heating limit of our measurements). Some inclusions decrepitated above 250 °C before homogenisation. Measured total homogenisation temperatures range from 260 to 380 °C, in most cases to the vapour phase (Fig. 17). Although entrapment at these high temperatures is consistent with the negative crystal shape of the inclusions, we are unsure how reliable measurements of homogenisation temperatures above 300 °C are given the presence of liquid hydrocarbons along the liquid–vapour interface. The oil phase retains its bright fluorescence even after heating to 400 °C with fluorescence colours becoming altered from yellow-cream to cream-orange.

5.3. Type 3 inclusions: light hydrocarbon and oil with water and a solid

These inclusions have up to four phases. They are generally between 10 and 20 μm in length, showing irregular shapes with a tendency towards sub-spherical morphologies. The inclusions occur in clusters, in isolation or within micro-fracture trails. Near-negative crystal forms occur in dense clusters of inclusions. A gas phase is always volumetrically dominant and typically forms 90% of the inclusion. Minor components variably include an outer rim of water, which is occasionally present at the interface between the gaseous phase and the host mineral, and either a thin rim of oil around the gas bubble or an oil globule within the aqueous phase. The inclusions are gener-

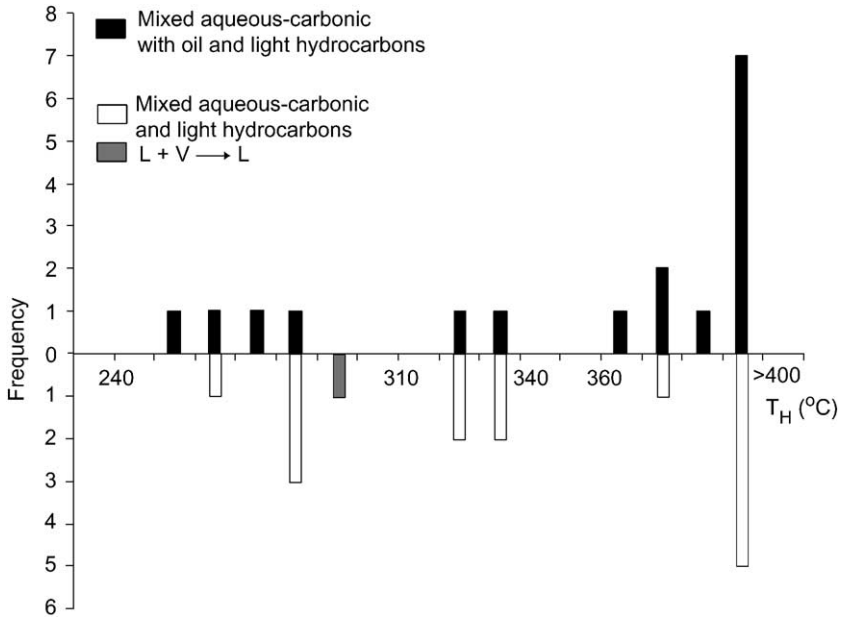

Fig. 17. Total homogenisation temperatures ($T_{H\ L+V \rightarrow L/V}$) for Type 2 mixed aqueous–carbonic inclusions.

ally very dark, largely due to a carbon coating at the inclusion–host interface making thermometric detection of CH_4 extremely difficult (Fig. 6E–F). No phase change was observed on cooling to −195 °C with liquid N_2. Laser Raman analysis reveals the presence of carbon, around 90 mol% CH_4, 8 mol% C_2H_6 and 2 mol% C_3H_8. No CO_2 was detected (Fig. 13E–F). The associated aqueous phase has very low salinity, which could not be accurately quantified using Mernagh and Wilde's (1989) method.

5.4. Type 4 inclusions: oil and gas

Type 4 inclusions are extremely rare, numbering 2 to 3 per standard thick section, and are isolated in their distribution. They comprise a fluorescent liquid phase (oil) around a gas bubble. These inclusions are generally quite small, measuring around 10 μm in length, and display irregular shapes. The combination of strong fluorescence, small size and low abundance prevents the analysis of these inclusions by spectroscopic methods. Consequently, it is not known whether the gaseous phase comprises hydrocarbon gases and/or CO_2. We have no microthermometric information on these inclusions.

6. Carbon isotope results

The $\delta^{13}C$ measurements are presented in Fig. 18 together with previous analyses of bitumen and kerogen carried out by Mossman et al. (1993a). The pyrobitumen nodules have the most depleted value of −25.6‰, the hydrocarbon gas from the fluid inclusions has a value of −24.9‰ and the bulk inclusion gas has the least depleted value of −16.2‰.

6.1. Interpretation

The $\delta^{13}C$ of the pyrobitumen nodules and hydrocarbon gas from the fluid inclusions falls within the range −25‰ to −33‰ for globular nodules in Elliot Lake as determined by Mossman et al. (1993a), suggesting a similar source. McKim Formation kerogen, a possible source, ranges from −22‰ to −27‰ while that of the overlying Pecors Formation, another possible source, is either markedly heavier or much lighter (Bekker et al., 1999). The values are also similar to the range expected for crude oils generated from organic matter and for thermogenic CH_4 (e.g. Fuex, 1977; Yeh and Epstein, 1981; Lewan, 1986) even after accounting for the effects of metamorphism (McKirdy and Powell,

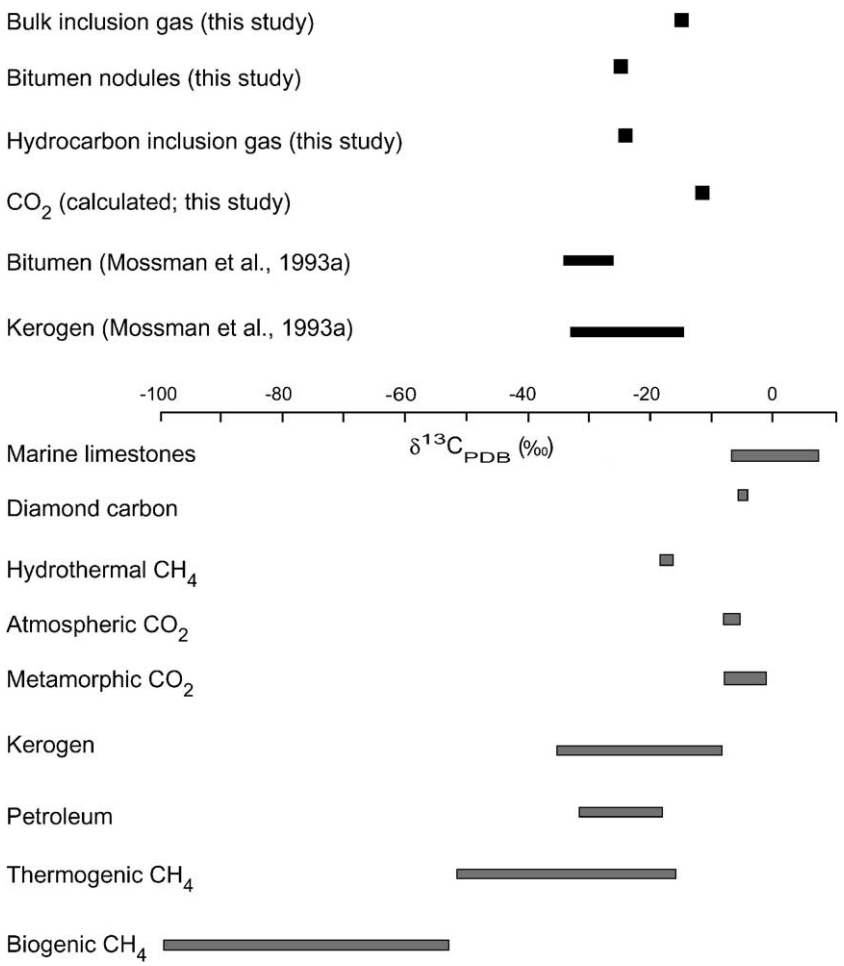

Fig. 18. $\delta^{13}C_{PDB}$ values of hydrocarbon and carbonic phases in the Matinenda Formation. Carbon isotope ratios of major carbon reservoirs are also shown.

1974) and radiation (Leventhal and Threlkeld, 1978). Consequently, the most likely ultimate source for the bitumen nodules and the hydrocarbon gas is biological debris in the McKim Formation.

From petrographic observations, it is evident that CO_2 forms about 95 vol.% of the bulk inclusion carbonic fluid with the remainder low molecular weight hydrocarbon gases (CH_4, C_2H_6 and C_3H_8). Based on the known $\delta^{13}C$ values of the hydrocarbon and bulk gases (Fig. 18) and bulk inclusion composition, the $\delta^{13}C$ of CO_2 should be around $-12‰$, considerably heavier than either the bulk gas or the hydrocarbons. The following sources and processes may account for this value.

(1) Generation of CO_2 through hydrous thermal alteration of organic matter in nearby mudstones and of petroleum in the pore space. In hydrous pyrolysis experiments CO_2 is the dominant volatile by-product produced directly from kerogen and bitumen over a range of thermal maturities. The amount of CO_2 released increases with increasing temperature and persists beyond peak hydrocarbon generation (Lewan, 1997; Seewald et al., 1998). From 65 to 95 mol% of the gas phase generated over time between 250 and 325 °C during a typical hydrous pyrolysis experiment is CO_2 (Seewald et al., 1998). These values are comparable to the CO_2 content of the gas phase of fluid inclusions trapped at similar temperatures in the

Matinenda Formation. Fluid hydrocarbons in the pore space would allow rapid in situ entrapment of an oil–CO_2 mixture in inclusions. Hunt (1996) indicated that thermal degradation of organic matter would typically produce CO_2 with $\delta^{13}C$ in the range of -8‰ to -12‰, which is similar to the calculated value for the CO_2 in our inclusions. Consequently, it is possible that the CO_2 in the inclusions has been produced by hydrous thermal alteration of solid and fluid hydrocarbons during the onset of metamorphism in the Matinenda Formation.

(2) CO_2 may have been generated through chemical oxidation of hydrocarbons by water (Pokrovskii, 1996) independent of temperature either within the inclusions or within the pore space. For example, McCollom (2001) has shown that toluene dissolved in water in the geological environment may undergo decarboxylation to CO_2 particularly in relatively oxidising solutions containing a high concentration of dissolved sulphur. At Elliot Lake, abundant pyrite and pyrrhotite would be suitable sources of sulphur. The reaction could proceed by hydrolytic disproportionation around 150 °C and 400 bars in a step-wise fashion as suggested by Helgeson et al. (1993) and would depend on the degree to which oil and water are in contact with each other. Some CH_4 would also be formed in this step-wise disproportionation, as is present in most oil-bearing CO_2 inclusions in the Matinenda Formation. In the fluid inclusions, the reactions could have taken place in a closed system over a period of more than 2 billion years and would thus not require elevated temperatures. The $\delta^{13}C$ of the resultant CO_2 should be very similar to the original hydrocarbons (Pankina, 1979). It is difficult to determine whether the inclusion CO_2 is more likely to come from generation in the pore space or is a post-entrapment alteration product within the inclusions. However, there are no pressure differences between inclusions containing oil and purely aqueous–carbonic inclusions (Fig. 19) and generation of large amounts of CO_2 in situ is therefore considered unlikely. But hydrolytic disproportionation could still have occurred in pore space with later inclusion entrapment, allowing $\delta^{13}C$ values of CO_2 to fractionate in the open system prevailing prior to inclusion sealing.

(3) CO_2 may have been generated by decarbonation reactions in surrounding carbonate rocks as the temperature increased towards peak metamorphism (sub-greenschist facies ca. 200–350 °C). Total homogenisation temperatures of the CO_2-rich inclusions indicate that CO_2 was mobile at high temperature ($\sim$ 250–350 °C). The $\delta^{13}C$ value of the CO_2 formed by this process should approximate the value of the carbonates (Hunt, 1996; Pankina, 1979). The Huronian sequence includes the Espanola Formation which comprises dolostones and limestones (Fig. 2) with $\delta^{13}C$ centred around -1.3‰ (Veizer et al., 1992) although $\delta^{13}C$ as low as -3.4‰ has been measured on the limestone (Schopf and Klein, 1992). Wycherley et al. (1999), however, suggested that contact metamorphism of carbonates, in this case by the ca. 2219 Ma Nipissing diabase, would result in ^{13}C depletions of derived CO_2 of about -6‰ with respect to the source carbonate. Consequently, only some Matinenda CO_2 could be derived from thermal alteration of carbonates, as such CO_2 should have been around -7‰ rather than -12‰.

(4) The CO_2 may have been derived from a magmatic source or other mantle source external to the Matinenda Formation. The Matinenda Formation was intruded by the Nipissing diabase ca. 2219 Ma, which may have supplied mantle-derived CO_2. In addition, the Matinenda Formation overlies or occurs close to the Archaean basement. In the Pannonian Basin, Hungary and in the Cooper–Eromanga Basin, Australia, the proximity of the basement is suspected to play a role in the supply of mantle-derived CO_2 to the reservoirs via deep-seated faults (Wycherley et al., 1999). The lower part of the Huronian Supergroup near Elliot Lake has experienced syn-depositional faulting (Young et al., 2001). Based on analyses of mid-ocean ridge basalts and diamonds, the $\delta^{13}C$ of the mantle CO_2 should be between -4‰ and -9‰ (e.g. Pineau and Javoy, 1983; Mattey et al., 1984; Deines, 1980). Thus, this could not have represented the sole source for the Matinenda CO_2.

The $\delta^{13}C$ values of the inclusion gases in the Matinenda Formation suggest that CO_2 could be derived from multiple sources. Only hydrous thermal alteration of hydrocarbon-rich substances, and possibly pore-space disproportionation, could produce the required $\delta^{13}C$ of the CO_2 without invoking a mixed source. However, based on carbon and noble gas isotope analyses of CO_2 in a variety of sedimentary basins, Wycherley et al. (1999) concluded that in general, large (>15 vol.%) accumulations of carbon dioxide cannot be explained exclusively by organically derived CO_2. If the Matinenda were not an

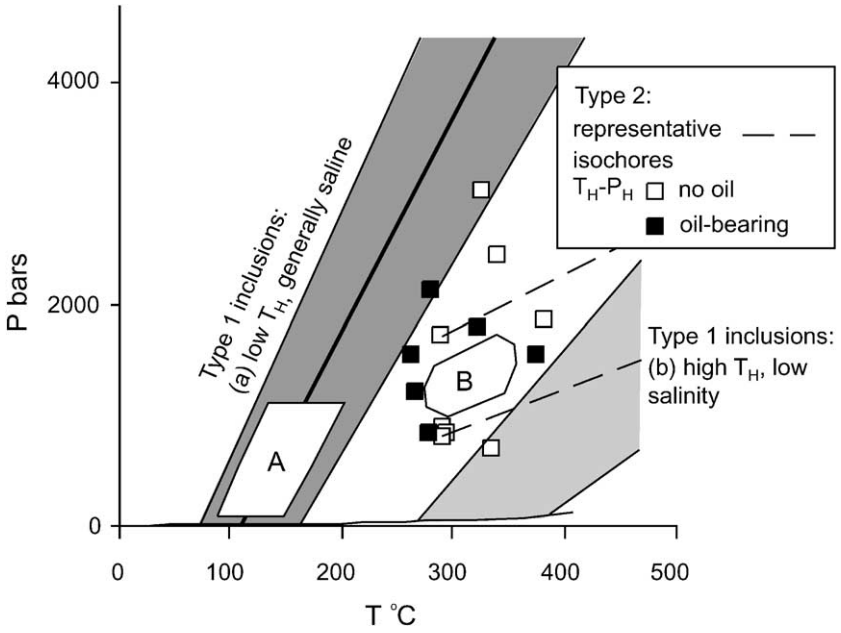

Fig. 19. Isochores and homogenisation temperatures and pressures of Type 1 and Type 2 oil-bearing inclusion types in the Matinenda Formation. Shaded bands show the range of isochores for Type 1 inclusions neglecting outliers. Thick solid line is the median isochore for the low T_H group of Type 1 inclusions. Polygons are interpreted conditions of two episodes of inclusion entrapment during diagenesis (A) and during very low-grade metamorphism (B). The equation of state of Bodnar and Vityk (1994) for the $H_2O-NaCl$ system and Kerrick and Jacobs (1981) adapted for the system $H_2O-CO_2-CH_4-NaCl$ were used in FLINCOR (Brown, 1989).

atypical reservoir, a mixed source of CO_2 is thus required. Consequently, fluid derived from inorganic sources (carbonates, mantle) would need to mix with biogenically derived CO_2 (thermally altered kerogen, oxidised oil) to produce $\delta^{13}C$ of $-12‰$ in the inclusion CO_2. However, given its ancient age, high metamorphic grade and complex history, a hydrous pyrolytic origin for Matinenda CO_2 cannot be excluded as a sole source.

7. Relative timing of hydrocarbon entrapment

The most common type of bitumen nodules in the Matinenda Formation are strikingly similar to those described from other Proterozoic sandstones (Buick et al., 1998), and consist of solid carbonaceous residues with inclusions of radioactive minerals. These types of nodules are formed by in situ irradiation originating from detrital radioactive U–Th-bearing minerals, interacting with fluid hydrocarbons as they flow through an interconnected pore network. Irradiation causes the hydrocarbons to polymerise and cross-link forming a highly viscous and ultimately solid residue around the radioactive mineral grains (Rasmussen, 1997). The shape and size of the nodules indicate that they have filled pre-existing intergranular pore space. As peak metamorphism would have occluded all remaining pore space and rendered the potential source rocks post-mature, the pyrobitumen nodules must have formed prior to peak metamorphism. Rare nodules containing non-radioactive sulphide minerals most likely formed by thermal alteration (e.g. Rogers et al., 1974) but likewise, their morphology suggests solidification within intergranular pore space.

Two periods of oil-bearing inclusion trapping during the diagenetic and metamorphic history of the Matinenda Formation can be deduced from the combined thermometric and textural data.

7.1. Early, low-temperature entrapment

The majority of Type 1 inclusions, in particular the high salinity sub-population, have features consistent

with entrapment at low temperatures early in burial history. Type 4 inclusions may also have been trapped at this stage. Homogenisation temperatures are dominantly between 80 and 200 °C, typical of the diagenetic environment of conventional reservoirs, and the isochore calculated for the median of the main mode of Type 1 inclusions passes through about 130 °C at 0.5 kbar and 200 °C at 2 kbar (Fig. 19). Most of these inclusions are dominated by a Na–Ca–Cl hypersaline brine with evidence of mixing with a low salinity fluid at low temperatures. Textural evidence shows that these oil-bearing inclusions were entrapped early in the burial history and before peak metamorphism. There are abundant inclusions in clearly diagenetic overgrowths to quartz grains (Fig. 5E–F). None of the fractures containing oil-bearing inclusions cross present-day grain boundaries and, where imaging by SEM-CL is possible, show random orientations within each quartz grain and truncation at grain boundaries (Fig. 3). These patterns are typical of brittle deformation during cementation and compaction of sandstone at relatively low temperature and pressure (Groshong, 1988).

Some of the hydrocarbons were thus trapped in fluid inclusions in authigenically healed intra-granular fractures, as documented in other sandstones of similar age (Dutkiewicz et al., 1998). Dickinson and Milliken (1995) believe that brittle deformation and authigenic cementation are generally concurrent processes, which would ensure rapid entrapment of circulating fluids. Quartz cementation in sedimentary basins is widely accepted as occurring at shallow to intermediate depths (1–2 km) and low temperatures (Bjørlykke and Egeberg, 1993). The rare oil–gas Type 4 inclusions are similar to those common in more modern oil systems and indicate migration as a discrete hydrocarbon phase. Most oil-bearing inclusions are however aqueous dominated with less than 5% oil. Given the low solubility of oil in water at the conditions of entrapment (Munz, 2001), these inclusion compositions imply migration in a heterogeneous phase, possibly as an emulsion with the brine.

The early inclusions would have been heated with the host rock to sub-greenschist facies metamorphic temperatures. Stretching of inclusions during metamorphism explains the rare high homogenisation temperatures (Figs. 11 and 12). The predominantly orange fluorescence of oils in these inclusions indicates substantial compositional modification of the hydrocarbons (e.g. George et al., 2001), either while migrating or after entrapment. The presence of bitumen and of mixed fluorescence colours in coeval inclusions suggests that the oil has undergone variable degrees of modification in different inclusions and hence that modification post-dates inclusion entrapment. As the oil was trapped with H_2O, its oxidation over an extended period of time should lead to molecular fractionation and a shift in fluorescence colours towards the red end of the visible colour spectrum (George et al., 2001). Recrystallisation during low-grade metamorphism has been recognised as the primary mechanism causing the migration of fluid inclusions onto subgrain boundaries (Kerrich, 1976), which is evident in the recrystallised portions of the Matinenda Formation but not within preserved portions of original quartz grains (Fig. 5G–H).

7.2. High temperature entrapment

The second major phase of oil-bearing fluid entrapment most likely occurred during metamorphism at entrapment temperatures of around 300 °C. Type 2 inclusions, low-salinity Type 1 inclusions with high homogenisation temperatures and possibly Type 3 inclusions have characteristics indicating entrapment at high temperatures. Homogenisation temperatures and pressures of Type 2 inclusions scatter broadly within the range 280 to 350 °C at 1 to 1.5 kbar (Fig. 19). These conditions are at or just above the two-phase field for low salinity aqueous–carbonic inclusions, and are within the range estimated for peak metamorphism at Elliot Lake. The variable phase proportions and opposite modes of total homogenisation of some assemblages of Type 2 inclusions are consistent with heterogeneous trapping of these assemblages at the two-phase boundary. The high temperatures of homogenisation of some Type 1 inclusions fall within the same temperature range, but these inclusions would be at lower pressures (0.1 to 1 kbar) at this range of temperatures. The negative crystal shape of many of these inclusions is as expected for entrapment at relatively high temperatures. There are a number of reasons why the Type 2 inclusions are not Type 1 inclusions modified as a result of alteration of entrapped oil: (a) The salinities are lower than in Type 1 inclusions; (b) CO_2–CH_4 ratios are very variable and

generally too high for the carbonic phase to be cracked oil (Wycherley et al., 1999); and (c) the mixed carbonic–aqueous fluids would not be stable as a single fluid at diagenetic conditions. Most of these inclusions are in microfractures restricted to individual quartz grains. Host microfractures are restricted to relatively undeformed portions of the quartz grains and do not cross present-day grain boundaries, indicating entrapment relatively early in the metamorphic and deformation history. The oil-bearing Type 2 inclusions have a very constant 2–3 vol.% oil. At temperatures of 300 to 350 °C, this amount of hydrocarbon would likely be soluble in CO_2-saturated water (Price, 1981). It is therefore conceivable that oil migrated as a molecular solution. Alternatively it could have migrated as a heterogeneous fluid. If this were the case, then Type 2 and Type 3 inclusions could represent a heterogeneously trapped CO_2–hydrocarbon–H_2O mixture. Further work involving infrared spectroscopy is required to fully characterise these inclusions, particularly with respect to CO_2 contents.

The same rocks responsible for supplying hydrocarbons to the low-temperature inclusions may have also supplied the high-temperature entrapment episode, as hydrous metamorphism could have facilitated the extraction of additional hydrocarbons following the initial diagenetic expulsion. Hydrous pyrolysis experiments (e.g. Lewan, 1997) indicate that hot aqueous solutions can generate significant quantities of fresh hydrocarbons from post-mature kerogen, so it is conceivable that a similar process could have operated here. The presence of voluminous CO_2 phases in these inclusions supports such an origin, as it could represent the residuum of the reaction:

$$2C + 2H_2O \rightarrow CH_4 + CO_2.$$

8. Origin of the inclusion CO_2

The total homogenisation temperatures of the CO_2–oil–water inclusions point towards a relatively hot fluid (~ 300 °C), which may result from any of the mechanisms described earlier to generate CO_2. The isotope compositions suggest that the CO_2 may have been derived from both organic and inorganic sources. In most oil-bearing fluid inclusions studied to date, CO_2 is usually present in relatively small amounts where it may be detected by FTIR (Cathelineau et al., 1997) and synchrotron FTIR (Guilhaumou et al., 1997, 2000) and is not obvious during visual inspection. However, these samples are from relatively shallow depths in conventional reservoirs, which are unlikely to have experienced temperatures above about 180 °C. The process responsible for high CO_2 content (up to 95 vol.%) in high-temperature oil-bearing inclusions may be unique to terrains which have experienced metamorphic temperatures during hydrocarbon migration. Data from natural gases and other fluid inclusions lead us to this conclusion. Very few natural gases in Phanerozoic sedimentary basins contain >10 mol% CO_2 (Imbus et al., 1998; Wycherley et al., 1999), but those that do are usually from a hot inorganic source. In the Greater Sleipner field in Norway, samples from 3.9 km contain up to 35 mol% CO_2 (James, 1990) apparently derived from thermal degradation of carbonates. In the Delaware–Val Verde basins of New Mexico and Texas, CO_2 is of volcanic origin (Holmquest, 1965). In southeast Asian reservoirs, the CO_2 abundance varies between 10 and 90 vol.% with a marked increase in CO_2 abundance at higher temperatures (e.g. Imbus et al., 1998; Smith and Ehrenberg, 1989; Franks and Forester, 1984; James and Burns, 1984). In fluid inclusions, Hoffmann et al. (1988) reported the presence of CO_2–water inclusions associated with high molecular weight hydrocarbons in a tin–tungsten deposit in Tasmania. The CO_2 was thought to have originated from mixed magmatic and non-magmatic sources and the inclusions homogenise between 300 and 450 °C. However, the complex hydrocarbons were not detected in individual inclusions. Furthermore, CO_2 is a common component of fluid inclusions in low to medium-grade metamorphic rocks (Roedder, 1984; Kruelen, 1980) where it can range from < 1 to 99 mol% and originate by a variety of processes, particularly the devolatilisation of organic matter and carbonates. Interestingly, the Witwatersrand Basin is the only other sedimentary basin known to us where visible CO_2 and oil co-exist within single inclusions (Dutkiewicz et al., 1998). The host rocks have likewise been metamorphosed to greenschist facies, but the CO_2–oil inclusions are not as large nor as diverse and are thus less amenable to microthermometric analysis. Hence, the Matinenda CO_2–oil inclusions represent the best-constrained occurrence of this assemblage so far known.

9. High temperature entrapment of complex hydrocarbons

The presence of oil in inclusions in the Matinenda Formation, which were evidently trapped between 250 and 330 °C, challenges the widely held view that oil becomes unstable and decomposes to methane and pyrobitumen by the end of the late catagenesis stage (~ 150–175 °C) (Tissot and Welte, 1984; Hayes, 1991; Hunt, 1996; Waples, 2000). The oil in the Matinenda Formation may have been carried in solution; however, irrespective of the mode of migration, it must have either been generated at high temperatures or have remigrated from a pre-existing reservoir with high-temperature aqueous–carbonic fluids. Many recent studies, mostly based on unconventional pyrolysis experiments, have been conducted to more accurately determine the stability limits of oil and the influence of parameters such as pressure, mineral catalysts, the presence of water, reaction kinetics and system closure. These have found that petroleum can survive at temperatures considerably higher than previously thought. Geochemical evidence for greater thermal stability of petroleum includes studies of aromatic compounds, which Kissin (1998) estimated to be stable at temperatures up to 300 °C. Using isothermal pyrolysis, Planche (1996) suggested that hydrocarbons may survive between 300 and 350 °C for as long as 100 million years and Price and Schoell (1995) demonstrated the presence of C_{2+} hydrocarbons at temperatures around 400 °C. Evidence from nature for greater thermal stability over geologically significant periods of time is also becoming more abundant. For example, Sajgó (2000) found that crude oils from Eastern Hungary were probably generated above 215 °C and suggested that the local temperature window for oil genesis was 100–300 °C with most generated between 130 and 250 °C. The best evidence for hydrocarbon stability should come from fluid inclusions and here too the evidence for high temperature entrapment is growing. Aliphatic hydrocarbons have been found preserved in fluid inclusions trapped at around 250 °C (Guilhaumou, 1982) and fluorescing hydrocarbons implying the presence of aromatic compounds occur in inclusions in rocks later heated to 300 °C (Dutkiewicz et al., 1998). Probably the highest temperature (300–450 °C) experienced, albeit briefly, by long-chained hydrocarbons in fluid inclusions is found in Devonian hydrothermal quartz veins (Hoffmann et al., 1988). The data from the Matinenda Formation supports the inferences from such studies that oil can be preserved to temperatures of this range, and may migrate at these temperatures. So it seems that, under certain circumstances, oil can survive thermal trauma considerably more intense than conventional wisdom suggests.

10. Implications for geological survival of hydrocarbons

This study has implications for the longevity of hydrocarbon molecules in geological environments. Oil trapped in the earlier population of inclusions in the Matinenda Formation has survived since the Palaeoproterozoic despite heating to metamorphic temperatures. Moreover, the fact that hydrocarbons in the Matinenda Formation still fluoresce indicates that aromatic molecules can survive under high temperatures for over 2 billion years. Similarly, the detection by laser Raman spectroscopy of several mol% propane in some high-temperature inclusions demonstrates that aliphatic chains can also persist under such conditions. This adds to a growing set of evidence that hydrocarbons may have greater temporal stability than once supposed. Long-chained hydrocarbons have survived at minimum temperatures of 225–260 °C for more than 300 million years while diluted hydrocarbons have been found at 250–350 °C (Price, 1993; Price and DeWitt, 2001). Experiments carried out by Dominé et al. (1998) predicted that the half-life of pure hexane under geological conditions is almost 1 billion years at 180 °C, becoming shorter at higher temperatures. Similarly, Mango (1991) suggested that the cycloalkane ring may be stable for billions of years under catagenic conditions.

From the fluid inclusion evidence, it is apparent that two factors probably played an important part in the extremely long stability of oil in the Matinenda Formation: (1) pressure, and (2) a closed system. The calculated pressures during entrapment of the CO_2–oil inclusions (0.5–2 kbar) are higher than conventional reservoirs which have pressures on the order of 250 bars (e.g. Benchilla et al., 2001; Teinturier and Pironon, 2001). Pyrolysis experiments suggest that

high fluid pressures hinder the maturation of petroleum (Dominé, 1991; Price and Wenger, 1992; Price, 1993). In nature, hydrocarbons have been found to survive high temperatures (190 °C) at relatively high pressures (1100 bar) in the North Sea (Vandenbroucke et al., 1999), while Sajgó et al. (1986) found that high load pressures (1–2 kbar) retarded maturation reactions at 250–400 °C in a semi-closed system. Giggenbach (1997) suggests that in closed systems, where there is no interaction between the hydrocarbon and rock, hydrocarbons generate their own redox environment and remain stable to much higher temperatures than in an open system. This is regarded as the critical factor for the preservation of oil in quartz-hosted inclusions in the Matinenda Formation.

11. Conclusions

Pyrobitumen nodules and oil-bearing fluid inclusions in the Palaeoproterozoic Matinenda Formation indicate hydrocarbon migration during burial diagenesis and also during early metamorphism ca. 2.2 Ga. Two populations dominate the oil-bearing fluid inclusions. The first comprises aqueous-oil inclusions located within original detrital grains and clasts and within rare quartz overgrowths. The second comprises aqueous–carbonic inclusions with a minor oil phase, light hydrocarbons and solids, which are located within microfractures in detrital quartz grains and clasts. In the first, oil was trapped at diagenetic temperatures and pressures ranging from 80 to 200 °C at less than 2 kbar in the presence of a high salinity fluid. In contrast, low-salinity aqueous–carbonic-oil inclusions were trapped at temperatures and pressures ranging from 280 to 350 °C and 1 to 1.5 kbar. High temperature entrapment of these inclusions is evident in their negative crystal shapes. $\delta^{13}C$ of pyrobitumen nodules and fluid inclusion hydrocarbon gas indicates a biogenic origin for the petroleum, whereas $\delta^{13}C$ of the bulk inclusion gas suggests that the carbonic phase is derived from mixed inorganic–organic CO_2 sources. Fluid inclusions in the Matinenda Formation thus yield direct evidence for prolonged survival of complex hydrocarbons under geological conditions that reached temperatures of low-grade metamorphism. This provides hope that organic geochemical analysis can extend into regions previously inaccessible to such investigations and suggests that deep, hot and/or old formations may not be completely devoid of potential for petroleum exploration, provided that good quality reservoirs and traps still exist.

Significant questions remaining from this study concern the extent of hydrocarbon entrapment and preservation in the Matinenda and adjacent formations, and the nature of the whole petroleum system of which only part of the migration pathway is recorded in the nodules and inclusions described here. Further work will involve the study of biomarker molecules in the oil inclusions and in probable source rocks from the Huronian section. Molecular characterization of the oils should also provide further insights on the thermal stability of specific hydrocarbon compounds, particularly aromatics about which very little is known under geologically extreme conditions. Characterisation will also help us determine whether oil was altered and oxidised in the inclusions and if so, to what extent. It would also be of interest to ascertain whether the oil in the two phases of migration was related genetically.

Acknowledgements

We thank Mike Hailstone, Ontario Geological Survey at Sault Ste. Marie, for providing drill-core access and advice on sampling localities, Terry Mernagh for help with laser Raman analysis, Birger Rasmussen for SEM-CL petrography, Anita Andrew and Brad McDonald for carbon isotope analysis, Peter Eadington for access to the CSIRO heating–freezing stage, and George Navratil for sample preparation. Constructive reviews of the original manuscript and ideas for further research by N. Guilhaumou and D. Mossman are greatly appreciated. This work was supported by ARC Grants A00103976 and F10009045. **[RR]**

References

Bekker, A., Eriksson, K.A., Kaufman, A.J., Karhu, J.A., Beukes, N.J., 1999. Paleoproterozoic record of biogeochemical events and ice ages. Abstr. Programs-Geol. Soc. Am. 31, 487.

Benchilla, L., Guilhaumou, N., Mougin, P., Jaswal, T., Roure, F., 2001. In: Noronha, F., Dória, A., Guedes, A. (Eds.), Proceed-

ings of the XVI European Current Research on Fluid Inclusions. Universidade do Porto, Faculdade de Ciências, Departamento de Geologia, pp. 37–39, Memórias No. 7.

Bjørlykke, K., Egeberg, P.K., 1993. Quartz cementation in sedimentary basins. AAPG Bull. 77, 1538–1548.

Bodnar, R.J., 1993. Revised equation and table for determining the freezing point depression of H_2O–NaCl solutions. Geochim. Cosmochim. Acta 57, 683–684.

Bodnar, R.J., Vityk, M.O., 1994. Interpretation of microthermometric data for H_2O–NaCl fluid inclusions. In: De Vivo, B., Frezzotti, M.L. (Eds.), Fluid Inclusions in Minerals: Methods and Applications. Short Course of the Working Group (IMA), Virginia Tech, Blacksburg, pp. 117–130.

Brown, P.E., 1989. FLINCOR: a microcomputer program for reduction and investigation of fluid inclusion data. Am. Mineral. 74, 1390–1393.

Buick, R., Rasmussen, B., Krapez, B., 1998. Archean oil: evidence for extensive hydrocarbon generation and migration 2.5–3.5 Ga. AAPG Bull. 82, 50–69.

Burruss, R.C., 1981. Hydrocarbon fluid inclusions in studies of sedimentary diagenesis. In: Hollister, L.S., Crawford, M.L. (Eds.), Fluid Inclusions, Applications to Petrology. Short Course Handbook, vol. 6. Mineralogical Association of Canada, Toronto, Canada, pp. 138–156.

Burruss, R.C., 1991. Practical aspects of fluorescence microscopy of petroleum fluid inclusions. In: Barker, C.E., Kopp, O.C. (Eds.), Luminescence Microscopy: Quantitative and Qualitative Aspects. SEPM Short Course Notes, vol. 25. Society of Sedimentary Geology, Tulsa, USA, pp. 1–7.

Card, K.D., 1978. Metamorphism of the middle Precambrian (Aphebian) rocks of the eastern Southern Province. In: Fraser, J.A., Heywood, W.W. (Eds.), Metamorphism in the Canadian Shield. Geol. Surv. Can. Paper, vol. 78-10, pp. 269–282.

Cathelineau, M., Banks, D., Ayt Ougougdal, M., Pironon, J., Boiron, M.C., Dubessy, J., Yardley, B., 1997. Fluid mixing during brine and oil migration in the Rhine Graben (Soultz deep drilling) at the basement-sedimentary cover contact; new fluid chemistry data. In: Boiron, M.C., Pironon, J. (Eds.), Proceedings of the XIV European Current Research on Fluid Inclusions. CNRS-CREGU, Nancy, France, pp. 60–61.

Cortial, F., Gauthier-Lafaye, F., Lacrampe-Couloume, G., 1990. Characterization of organic matter associated with uranium deposits in the Francevillian Formation of Gabon (Lower Proterozoic). Org. Geochem. 15, 73–85.

Dahlkamp, F.J., 1993. Uranium Ore Deposits. Springer-Verlag, Berlin, Germany, 460 pp.

Deines, P., 1980. The carbon isotopic composition of diamonds: relationship to diamond shape, color, occurrence and vapor composition. Geochim. Cosmochim. Acta 44, 943–961.

Diamond, L.W., 1992. Stability of CO_2 clathrate hydrate + CO_2 liquid + CO_2 vapour + aqueous KCl–NaCl solutions: experimental determination and application to salinity estimates of fluid inclusions. Geochim. Cosmochim. Acta 56, 273–280.

Dickinson, W.W., Milliken, K.L., 1995. The diagenetic role of brittle deformation in compaction and pressure solution, Etjo Sandstone, Namibia. J. Geol. 103, 339–347.

Dominé, F., 1991. High pressure pyrolysis of *n*-hexane 2,4-dimethylpentane and 1-phenylbutane. Is pressure an important geochemical parameter? Org. Geochem. 17, 619–634.

Dominé, F., Dessort, D., Brévart, O., 1998. Towards a new method of geochemical kinetic modelling: implications for the stability of crude oils. Org. Geochem. 28, 597–612.

Dutkiewicz, A., Rasmussen, B., Buick, R., 1998. Oil preserved in fluid inclusions in Archaean sandstones. Nature 395, 885–888.

Fralick, P.W., Miall, A.D., 1989. Sedimentology of the Lower Huronian Supergroup (Early Proterozoic), Elliot Lake area, Ontario, Canada. Sediment. Geol. 63, 127–153.

Franks, S.G., Forester, R.W., 1984. Relationships among secondary porosity, pore-fluid chemistry and carbon dioxide, Texas Gulf Coast. AAPG Mem. 37, 63–79.

Fuex, A.N., 1977. The use of stable carbon isotopes in hydrocarbon exploration. J. Geochem. Explor. 7, 155–188.

George, S.C., Llorca, S.M., Hamilton, P.J., 1994. An integrated analytical approach for determining the origin of solid bitumens in the McArthur Basin, northern Australia. Org. Geochem. 21, 235–248.

George, S.C., Ruble, T.E., Dutkiewicz, A., Eadington, P.J., 2001. Assessing the maturity of oil trapped in fluid inclusions using molecular geochemistry data and visually-determined fluorescence colours. Appl. Geochem. 16, 451–473.

Giggenbach, W.F., 1997. Relative importance of thermodynamic and kinetic processes in governing the chemical and isotopic composition of carbon gases in high-heatflow sedimentary basins. Geochim. Cosmochim. Acta 61, 3763–3785.

Goldstein, R.H., Reynolds, T.J., 1994. Systematics of Fluid Inclusions in Diagenetic Minerals. SEMP (Society of Sedimentary Geology) Short Course, vol. 31, 199 pp.

Groshong, R.H., 1988. Low-temperature deformation mechanisms and their interpretation. Geol. Soc. Amer. Bull. 100, 1329–1360.

Guilhaumou, N., 1982. Precise analysis of fluid inclusions by laser molecular microprobe (Mole) and microthermometry. Trav. Lab. Geol., Ec. Norm. Super. 14 (88 pp.).

Guilhaumou, N., Dumas, P., Carr, G.L., Williams, G.P., 1997. In: Boiron, M.C., Pironon, J. (Eds.), Proceedings of the XIV European Current Research on Fluid Inclusions. CNRS-CREGU, Nancy, France, pp. 142–143.

Guilhaumou, N., Ellouz, N., Jaswal, T.M., Mougin, P., 2000. Genesis and evolution of hydrocarbons entrapped in the fluorite deposit of Koh-i-Maran (North Kirthar Range, Pakistan). Mar. Pet. Geol. 17, 1151–1164.

Hayes, J.M., 1991. Geochemistry: stability of petroleum. Nature 352, 108–109.

Helgeson, H.C., Knox, A.M., Owens, C.E., Shock-Everett, L., 1993. Petroleum, oil field waters, and authigenic mineral assemblages: are they in metastable equilibrium in hydrocarbon reservoirs? Geochim. Cosmochim. Acta 57, 3295–3339.

Hoefs, J., Stalder, H.A., 1977. Carbon isotopic composition of CO_2 from fissure quartz of the Central Alps. Schweiz. Mineral. Petrogr. 57, 329–347.

Hoffmann, C.F., Henley, R.W., Higgins, N.C., Solomon, M., Summons, R.E., 1988. Biogenic hydrocarbons in fluid inclusions from the Aberfoyle tin–tungsten deposit, Tasmania, Australia. Chem. Geol. 70, 287–299.

Holmquest, H.J., 1965. Deep plays in Delaware and Val Verde

basins. In: Young, A., Galley, J.E. (Eds.), Fluids in Subsurface Environments. AAPG Mem., vol. 4, pp. 257–279.

Hu, Q., Evensen, N.M., Smith, P.E., York, D., 1998. A world in a grain of sand: regional metamorphic history from $^{40}Ar/^{39}Ar$ laser probe analyses of Proterozoic sediments from the Canadian Shield. Precambrian Res. 91, 287–294.

Hunt, J.M., 1996. Petroleum Geochemistry and Geology. Freeman, New York. 743 pp.

Imbus, S.W., Katz, B.J., Urwongse, T., 1998. Predicting CO_2 occurrence on a regional scale: southeast Asia example. Org. Geochem. 29, 325–345.

James, A.T., 1990. Correlation of reservoired gases using the carbon isotopic composition of wet gas components. AAPG Bull. 74, 1441–1448.

James, A.T., Burns, B.J., 1984. Microbial alteration of subsurface natural gas accumulations. AAPG Bull. 68, 957–960.

Kaiman, S., Horwood, J.L., 1976. An unusual "thucholite" from Elliot Lake, Ontario. Can. Mineral. 14, 422–428.

Kelly, W.C., Nishioka, G.K., 1985. Precambrian oil inclusions in late veins and the role of hydrocarbons in copper mineralization at White Pine, Michigan. Geology 13, 334–337.

Kerrich, R., 1976. Some effects of tectonic recrystallization on fluid inclusions in vein quartz. Contrib. Mineral. Petrol. 59, 195–202.

Kerrick, D.M., Jacobs, G.K., 1981. A modified Redlich–Kwing equation for H_2O, CO_2 and $H_2O–CO_2$ mixtures at elevated pressures and temperatures. Am. J. Sci. 281, 735–767.

Kissin, Y.V., 1998. Catagenesis of light aromatic compounds in petroleum. Org. Geochem. 29, 947–962.

Krogh, T.E., Davis, D.W., Corfu, F., 1984. Precise U–Pb zircon and baddeleyite ages of the Sudbury area. In: Pye, E.G. (Ed.), Geology and Ore Deposits of the Sudbury Structure. Ontario Geological Survey, Special Volume 1, pp. 431–446.

Kruelen, R., 1980. CO_2-rich fluids during regional metamorphism on Naxos (Greece): carbon isotopes and fluid inclusions. Am. J. Sci. 280, 757–771.

Kvenvolden, K.A., Roedder, E., 1971. Fluid inclusions in quartz crystals from South-West Africa. Geochim. Cosmochim. Acta 35, 1209–1229.

Leventhal, J.S., Threlkeld, C.N., 1978. Carbon-13/carbon-12 isotope fractionation of organic matter associated with uranium ores induced by alpha irradiation. Science 202, 430–432.

Lewan, M.D., 1986. Stable carbon isotopes of amorphous kerogens from Phanerozoic sedimentary rocks. Geochim. Cosmochim. Acta 50, 1583–1591.

Lewan, M.D., 1997. Experiments on the role of water in petroleum formation. Geochim. Cosmochim. Acta 61, 3691–3723.

Mango, F.D., 1991. The stability of hydrocarbons under the time–temperature conditions of petroleum genesis. Nature 352, 146–148.

Mattey, D.P., Carr, R.H., Wright, I.P., Pillinger, C.T., 1984. Carbon isotopes in submarine basalts. Earth Planet. Sci. Lett. 70, 196–206.

McCollom, T.M., 2001. Reactivity of monocyclic aromatic compounds under hydrothermal conditions. Geochim. Cosmochim. Acta 65, 455–468.

McKirdy, D.M., Imbus, S.W., 1992. Precambrian petroleum: a decade of changing perceptions. In: Schidlowski, M., Golubic, S., Kimberley, M.M., McKirdy, D.M., Trudinger, P.A. (Eds.), Early Organic Evolution: Implications for Mineral and Energy Resources. Springer-Verlag, Berlin, pp. 177–192.

McKirdy, D.M., Powell, T.G., 1974. Metamorphic alteration of carbon isotopic composition in ancient sedimentary organic matter: new evidence from Australia and South Africa. Geology 2, 591–595.

McLennan, S.M., Simonetti, A., Goldstein, S.L., 2000. Nd and Pb isotopic evidence for provenance and post-depositional alteration of the Paleoproterozoic Huronian Supergroup, Canada. Precambrian Res. 102, 263–278.

Mernagh, T.P., Wilde, A.R., 1989. The use of laser Raman microprobe for the determination of salinity in fluid inclusions. Geochim. Cosmochim. Acta 53, 765–771.

Mossman, D.J., 1987. Stratiform gold occurrences of the Witwatersrand type in the Huronian Supergroup, Ontario, Canada. Trans. Geol. Soc. S.-Afr. 90, 168–178.

Mossman, D.J., Goodarzi, F., Gentzis, T., 1993a. Characterisation of insoluble organic matter from the Lower Proterozoic Huronian Supergroup, Elliot Lake, Ontario. Precambrian Res. 61, 279–293.

Mossman, D.J., Nagy, B., Davis, D.W., 1993b. Hydrothermal alteration of organic matter in uranium ores, Elliot Lake, Canada: implications for selected organic-rich deposits. Geochim. Cosmochim. Acta 57, 3251–3259.

Mossman, D.J., Gauthier-Lafaye, F., Jackson, S.E., 2001. Carbonaceous substances associated with the Paleoproterozoic natural nuclear fission reactors of Oklo, Gabon: paragenesis, thermal maturation and carbon isotopic and trace element compositions. Precambrian Res. 106, 135–148.

Munz, I.A., 2001. Petroleum inclusions in sedimentary basins: systematics, analytical methods and applications. Lithos 55, 195–212.

Oakes, C.S., Bodnar, R.J., Simonson, J.M., 1990. The system $NaCl–CaCl_2–H_2O$: I. The ice liquidus at 1 atm total pressure. Geochim. Cosmochim. Acta 54, 603–610.

Pankina, R.G., 1979. Origin of CO_2 in petroleum gases (from the isotopic composition of carbon). Int. Geol. Rev. 21, 535–539.

Parnell, J., 1996. Phanerozoic analogues for carbonaceous matter in Witwatersrand ore deposits. Econ. Geol. Bull. Soc. Econ. Geol. 91, 55–62.

Pineau, F., Javoy, M., 1983. Carbon isotopes and concentration in mid-oceanic ridge basalts. Earth Planet. Sci. Lett. 62, 239–257.

Planche, H., 1996. Finite time thermodynamics and the quasi-stability of closed-systems of natural hydrocarbon mixtures. Geochim. Cosmochim. Acta 22, 4447–4465.

Pokrovskii, V.A., 1996. The oxidative solubility of petroleum in formation waters: implications for hydrothermal transport, diagenesis, and development of secondary porosity in reservoir rocks. In: Kennard, J.M. (Ed.), Geoscience for the Community, 13th Australian Geological Convention. Geological Society of Australia, vol. 41, p. 347.

Price, L.C., 1981. Aqueous solubility of crude oil to 400 °C and 2000 bars pressure in the presence of gas. J. Pet. Geol. 4, 195–223.

Price, L.C., 1993. Thermal stability of hydrocarbons in nature: limits, evidence, characteristics and possible controls. Geochim. Cosmochim. Acta 57, 3261–3280.

Price, L.C., DeWitt, E., 2001. Evidence and characteristics of hydrolytic disproportionation of organic matter during metasomatic processes. Geochim. Cosmochim. Acta 65, 3791–3826.

Price, L.C., Schoell, M., 1995. Constraints on the origins of hydrocarbon gas from compositions of gases at their site of origin. Nature 378, 368–371.

Price, L.C., Wenger, L.M., 1992. The influence of pressure on petroleum generation and maturation as suggested by aqueous pyrolysis. Org. Geochem. 19, 141–159.

Rasmussen, B., 1997. Fluorescent growth bands in irradiation–bitumen nodules: evidence of episodic hydrocarbon migration. AAPG Bull. 81, 17–25.

Robertson, J.A., 1981. The Blind River uranium deposits: the ores and their setting. In: Armstrong, F.C. (Ed.), Genesis of Uranium and Gold-bearing Precambrian Quartz Pebble Conglomerates. U.S. Geol. Surv. Prof. Paper, pp. U1–U23.

Robinson, A.G., Spooner, E.T.C., 1984. Postdepositional modification of uraninite-bearing quartz–pebble conglomerates from the Quirke ore zone, Elliot Lake, Ontario. Econ. Geol. Bull. Soc. Econ. Geol. 79, 297–321.

Roedder, E., 1984. Fluid Inclusions. Reviews in Mineralogy, vol. 12. Mineralogical Society of America, Washington, DC. 646 pp.

Rogers, M.A., McAlary, J.D., Bailey, N.J.L., 1974. Significance of reservoir bitumens to thermal-maturation studies, West Canada Basin. AAPG Bull. 58, 1806–1824.

Roscoe, S.M., 1969. Huronian rocks and uriniferous conglomerates in the Canadian Shield. Geol. Surv. Can., Pap. 56-7 (205 pp.).

Sajgó, Cs., 2000. Assessment of generation temperatures of crude oils. Org. Geochem. 31, 1301–1323.

Sajgó, Cs., McEvoy, J., Wolff, G.A., Horváth, Z.A., 1986. Influence of temperature and pressure on maturation processes: I. Preliminary report. Org. Geochem. 10, 331–337.

Schopf, J.W., Klein, C., 1992. The Proterozoic Biosphere: A Multidisciplinary Study. University of Cambridge, Cambridge, UK. 1348 pp.

Seewald, J.S., Benitez-Nelson, B., Whelan, J.K., 1998. Laboratory and theoretical constraints on the generation and composition of natural gas. Geochim. Cosmochim. Acta 62, 1599–1617.

Smith, J.T., Ehrenberg, S.N., 1989. Correlation of carbon dioxide abundance with temperature in clastic hydrocarbon reservoirs: relationship to inorganic chemical equilibrium. Mar. Pet. Geol. 6, 129–135.

Spangenberg, J.E., Frimmel, H.E., 2001. Basin-internal derivation of hydrocarbons in the Witwatersrand Basin, South Africa: evidence from bulk and molecular $\delta^{13}C$ data. Chem. Geol. 173, 339–355.

Sutton, S.J., Maynard, J.B., 1993. Petrology, mineralogy, and geochemistry of sandstones of the lower Huronian Matinenda Formation: resemblance to underlying basement rocks. Can. J. Earth Sci. 30, 1209–1223.

Teinturier, S., Pironon, J., 2001. Quartz cementation and hydrocarbon emplacement examples from the Garn Formation, Haltenbanken, mid-Norway. In: Noronha, F., Dória, A., Guedes, A. (Eds.), Proceedings of the XVI European Current Research on Fluid Inclusions, pp. 431–433.

Theis, N.J., 1979. Uranium-bearing and associated minerals in their geochemical and sedimentological context, Elliot Lake, Ontario. Geol. Surv. Can., Bull. 304 (50 pp.).

Tissot, B.P., Welte, D.H., 1984. Petroleum Formation and Occurrence, 2nd ed. Springer-Verlag, Berlin, Germany. 699 pp.

Vandenbroucke, M., Behar, F., Rudkiewicz, J.L., 1999. Kinetic modelling of petroleum formation and cracking: implications from the high pressure/high temperature Elgin Field (UK, North Sea). Org. Geochem. 30, 1105–1125.

Veizer, J., Clayton, R.N., Hinton, R.W., 1992. Geochemistry of Precambrian carbonates: IV. Early Paleoproterozoic (2.25 ± 0.25 Ga) seawater. Geochim. Cosmochim. Acta 56, 875–885.

Vennemann, T.W., Kesler, S.E., Frederickson, G.C., 1995. Oxygen isotope sedimentology and uranium-bearing Witwatersrand and Huronian Supergroup quartz–pebble conglomerates. Econ. Geol. 91, 322–342.

Waples, D.W., 2000. The kinetics of in-reservoir oil destruction and gas formation: constraints from experimental and empirical data, and from thermodynamics. Org. Geochem. 31, 553–575.

Willingham, T.O., Nagy, B., Nagy, L.A., Krinsley, D.H., Mossman, D.J., 1985. Uranium-bearing stratiform organic matter in paleoplacers of the lower Huronian Supergroup, Elliot Lake–Blind River region, Canada. Can. J. Earth Sci. 22, 1930–1944.

Wycherley, H., Fleet, A., Shaw, H., 1999. Some observations on the origins of large volumes of carbon dioxide accumulations in sedimentary basins. Mar. Pet. Geol. 16, 489–494.

Yeh, H.W., Epstein, S., 1981. Hydrogen and carbon isotopes of petroleum and related organic matter. Geochim. Cosmochim. Acta 45, 753–762.

Young, G.M., 1981. Field guide to the sedimentary environments and regional tectonic setting of the Huronian Supergroup, north shore of Lake Huron, Ontario, Canada. 11th Annual Field Conference of the Great Lakes Section. Soc. Econ. Paleontol. Mineral. (62 pp.).

Young, G.M., Nesbitt, H.W., 1985. The Gowganda Formation in the southern part of the Huronian outcrop belt, Ontario, Canada: stratigraphy, depositional environments and regional tectonic significance. Precambrian Res. 29, 265–301.

Young, G.M., Long, D.G.F., Fedo, C.M., Nesbitt, H.W., 2001. Paleoproterozoic Huronian basin: product of a Wilson cycle punctuated by glaciations and meteorite impact. Sediment. Geol. 141–142, 233–254.